Transcriptomic and chromatin accessibility profiling unveils new regulators of heat hormesis in *Caenorhabditis elegans*

Author Information

Hsin-Yun Chang[1], Sarah E. McMurry[1], Sicheng Ma[1], Christian A. Mansour [1], Sophia Marie T. Schwab[1], Charles G. Danko[2], & Siu Sylvia Lee[1*]

Affiliations

[1]Department of Molecular Biology and Genetics, Cornell University, Ithaca, New York, United States of America

[2]Department of Biomedical Science, Cornell University, Ithaca, New York, United States of America

Correspondence: Siu Sylvia Lee (sylvia.lee@cornell.edu)

Abstract

Heat hormesis describes the beneficial adaptations from transient exposure to mild heat stress, which enhances stress resilience and promotes healthy aging. It is thought to be the underlying basis of popular wellness practices like sauna therapy. Despite extensive documentation across species, the molecular basis of the long-term protective effects of heat hormesis remain poorly understood. This study bridges that critical gap through a comprehensive multiomic analysis, providing key insights into the transcriptomic and chromatin accessibility landscapes throughout a heat hormesis regimen adapted in *C. elegans*. We uncover highly dynamic dose-dependent molecular responses to heat stress and reveal that while most initial stress-induced changes revert to baseline, key differences in response to subsequent heat shock challenge are directly linked to physiological benefits. We identify new regulators of heat hormesis, including MARS-1/MARS1, SNPC-4/SNAPc, ELT-2/GATA4, FOS-1/c-Fos, and DPY-27/SMC4, which likely orchestrate gene expression programs that enhance stress resilience through distinct biological pathways. This study advances our understanding of stress resilience mechanisms, points to multiple new avenues of future investigations, and suggests potential strategies for promoting healthy aging through mid-life stress management.

Keywords: Heat hormesis, stress adaptation, dose-dependent response*, Caenorhabditis elegans*, transcriptomic profiling, chromatin accessibility profiling.

Introduction

Transient exposure to mild stress is well known to activate adaptive mechanisms that confer long-term protective effects and promote health, a phenomenon known as hormesis[1–4]. Specifically, 'heat hormesis' describes the beneficial outcomes triggered by mild thermal stress, documented across species from yeast to human[4–13]. Sauna therapy, for instance, is increasingly recognized for its potential to improve health

and mitigate age-related diseases through mechanisms attributed to heat hormesis[14,15]. Despite broad observational evidence and growing popularity for wellness, the underlying mechanisms by which early-life exposure to mild heat stress confers memory-like protective effects are not fully understood.

In *C. elegans,* exposure to elevated temperatures during early life stages, including short exposures in young adulthood[4,6,16–19] or chronic exposure throughout development[20,21], consistently boosts thermal resistance and extends lifespan. Mechanisms underlying heat hormesis involve the heat shock transcription factor HSF-1, which mediates heat shock response and autophagy, as well as insulin/insulin growth factor-1 signaling pathways[10,17,19,22]. Recent studies highlighted the role of transcriptional and epigenetic memory in contributing to long-term beneficial effects. For instance, the SWI/SNF chromatin remodeling complex and the histone acetyltransferase CBP-1 have been implicated in maintaining persistent induction of innate immune genes, mediating stress adaptation and longevity following early-life heat exposure[21]. Furthermore, CBP-1 has been shown to regulate the gene tsp-1, encoding the tetraspanin protein that confers heat hormesis effects[23]. Another study demonstrated that the endoribonuclease ENDU-2 facilitate long-term protection through transcriptional reprogramming during the post-heat stress period[24].

Despite significant advances, a longitudinal multiomic analysis that tracks changes across the entire heat hormesis regimen, including subsequent stress re-challenge, remains unexplored. Such data could provide crucial molecular insights that correlate with the improved physiological outcomes observed under hormesis condition and point to possible regulators of the protective effects. Our study reported here fills this gap by presenting detailed transcriptomic and chromatin accessibility profiles at key timepoints throughout a heat hormesis regimen. By establishing a robust heat hormesis regimen where worms were exposed to a 6-hour "priming" at 30°C during early adulthood, we significantly enhanced their thermal resistance after a 12-hour recovery at normal growth temperature. This regimen allowed us to track extensive changes in RNA expression and chromatin accessibility that, although largely restored after the 12-hour recovery period, left distinct molecular imprints upon subsequent heat shocks (HS). Our findings

illustrated the dynamic molecular landscape during heat hormesis, providing concrete molecular evidence for dose-dependent responses and uncovering new regulators with critical roles in diverse biological functions. We identified MARS-1, linking methionine incorporation during protein synthesis to heat hormesis; SNPC-4, highlighting the importance of piRNA-mediated post-transcriptional regulation in stress response; ELT-2, suggesting that GATA factors integrate developmental cues and stress signals; FOS-1, part of the AP-1 pioneer transcription factor complex, suggesting a mechanisms for encoding heat hormesis memory through chromatin remodeling; and DPY-27, suggesting a link between dosage compensation complex-mediated chromosome architecture and heat stress management. Overall, this study provided a comprehensive view of transcriptional and chromatin dynamics during heat hormesis, offering valuable insights into the molecular basis of developing stress resilience and may pave the way for healthy aging through stress management.

Results and Discussion

Priming induces thermal-resistance and lifespan extension

To understand the molecular basis of heat hormesis, we adapted a regimen where *C. elegans* that have been cultured at 20°C were exposed to 30°C for 6 hours during early adulthood (referred to as 'priming'), allowed to recover at 20°C, and were then either re-challenged with heat shock (HS) at 35°C or 37°C or aged at 20°C. We applied this hormesis regimen to wild-type (WT) or *glp-1(e2141)* mutant (referred to as *glp-1(ts)* hereafter), which become germlineless when grown at the non-permissive temperature of 25°C, and tested their thermal-resistance after HS or their longevity under normal culturing temperature.

We found that priming significantly improved thermal-resistance, based on motility scoring, in WT and *glp-1(ts)* mutant and the enhanced thermal-resistance persisted after 12- or 48-hours of recovery at 20°C (Fig. 1c, Supplementary Fig. 1a), but the effect waned after a 96-hour recovery period. These results

indicated that both WT and *glp-1(ts)* worms can retain a "memory" of the priming experience for an extended period of time, thereby exhibiting enhanced resistance to subsequent HS challenge. In addition, we monitored survival of *glp-1(ts)* worms after 3 or 6 hours of HS and observed that the primed worms with 12-hour recovery lived substantially longer than their naive counterparts (Fig. 1d, e). Moreover, we tested varying priming period and determined that a 6-hour priming showed substantially greater protective effect compared to shorter priming time (Supplementary Fig. 1c).

We next investigated lifespan post priming and found that priming at 30°C for 6 hours on first day of adulthood consistently extended the lifespan of WT worms (Supplementary Fig. 1b), corroborating previous reports [6,16]. Interestingly, our priming regimen did not extend lifespan in the *glp-1(ts)* mutant (Fig. 1b). The *glp-1(ts)* mutant is well-established to be long-lived compared to WT (Fig. 1b, naive group), but priming at 30°C for 6 hours during early adulthood did not further impact their lifespan (Fig. 1b, primed group). We observed that priming primarily impacted the mean and median lifespan of WT worms rather than the maximum lifespan, suggesting that priming may decrease lifespan variability between individuals[25]. This resembles findings from previous studies where transient reactive oxygen species (ROS) stress during development confers stress resistance and longer lifespan in *C. elegans*[26].

In exploring how priming might impact lifespan differently in WT and *glp-1(ts)* mutant, we demonstrated that priming resulted in a small but significant reduction in total brood size in the primed WT compared to the naive worms, with the majority of reduction occurring during the priming period and within 12 hours after priming (Supplementary Fig. 1d, e; Supplementary text). It is well known in the field that ablation of germline stem cells, or a genetic mimic such as the *glp-1(ts)* mutation, is able to significantly extend *C. elegans* lifespan. It is therefore possible that a transient compromising effect on germline development during the 6 hours of priming is sufficient to induce a pro-longevity signal in WT. It is also possible that the pro-longevity mechanisms that are induced by priming are already manifested in the germlineless *glp-1(ts)* mutant, thus priming is not able to further increase its lifespan. Future investigation to distinguish between priming-related and reproductive-related factors contributing to longevity will likely be fruitful.

Transcriptomic and chromatin accessibility profiling in heat hormesis

To investigate the molecular basis of how transient exposure to mild heat stress, i.e. priming, confers resistance to a more intense heat stress later, we profiled mRNA expression and chromatin accessibility using RNA-seq and ATAC-seq at key timepoints across our heat hormesis regimen. We hypothesized that RNA-seq and ATAC-seq data together would provide a more comprehensive view of the dynamics of gene expression regulation across the heat hormesis regimen. We employed the *glp-1(ts)* strain to simplify the interpretation of the genomic data, as germline cells in WT undergo extensive transcriptional reprogramming during the active reproductive period in the early adult stage. The timepoints we chose, including immediately after the 6-hour priming at 30°C (timepoint 1), after the 12-hour recovery at 20°C (timepoint 2), and after 3 or 6 hours of HS at 35°C (timepoint 3) (Fig. 1a), were guided by the dramatic phenotypic differences between primed and naive *glp-1(ts)* worms after HS at 35°C (Fig. 1d, e).

We first examined how RNA expression and chromatin accessibility change across the heat hormesis regimen in the naive group. We detected only minior changes at timepoints 1 and 2 (N1 vs NC, N2 vs N1) (Supplementary Fig. 3a), likely reflecting developmental progression over the periods of 6 and 12 hours at normal culturing temperature. HS at 35°C for 3 or 6 hours induced dramatic changes both in RNA expression and in chromatin accessibility (N3 vs N2) (Supplementary Fig. 3a; *source.data*); These changes showed significant overlap with previously reported heat stress-induced gene expression changes (Supplementary Fig. 3e; *source.data*)[24,27], despite differences in experimental setup, supporting the validity of our results.

Priming-responsive changes largely restore after recovery

We next focused our analyses on the primed group. RNA-seq analysis revealed substantial RNA expression changes following priming (P1 vs NC). Specifically, RNA expression of 1,390 and 1,423 genes were significantly up- or down-regulated respectively after priming (Fig. 2a, Supplementary Fig. 3b). After a 12-hour recovery at 20°C, significant RNA expression changes were again detected (P2 vs P1), with 1,237 and 1,136 genes up- or down-regulated (Fig. 2a, Supplementary Fig. 3b). Intriguingly, 837 genes that were upregulated immediately after priming showed significantly reduced expression after recovery, and 900 genes initially downregulated in response to priming showed significantly increased expression after recovery (Fig. 2a, Supplementary Fig. 3b). These results indicated that while priming induces significant changes in RNA expression, the majority of these changes were transient and largely restored after a recovery period.

ATAC-seq analysis also revealed significant changes in chromatin accessibility after priming (P1 vs NC), with 808 peaks and 2,110 peaks showing significant up- or down-regulation, respectively (Fig. 2b, Supplementary Fig. 3b). Following the recovery period (P2 vs P1), chromatin accessibility significantly increased at 1,135 peaks and decreased at 437 peaks Fig. 2b, Supplementary Fig. 3b). Among those that showed significant changes after priming (P1 vs NC) or after recovery (P2 vs P1), we observed that 284 peaks that gained accessibility immediately after priming exhibited reduced accessibility after recovery, and 819 peaks that were less accessible post-priming regained accessibility after recovery (Fig. 2b, Supplementary Fig. 3b). Although a simple intersection among the significantly changed peaks after priming and after recovery suggested a large number of non-overlapping peaks, e.g. red (524) or blue (1291) portion of the Venn diagram in Fig. 2b, a closer inspection of the data indicated that those seemingly unique peaks (in the non-overlapping regions of the Venn diagram) nevertheless exhibited accessibility changes in the opposing direction at P1 and P2, albeit not reaching significance. We interpreted these results to suggest that most chromatin accessibility changes induced by priming are restored after a recovery period, similar to the dynamic response of the transcriptome to priming.

Upon HS at 35°C for 3 or 6 hours, we observed dramatic changes in RNA expression and chromatin accessibility in the primed group (Supplementary Fig. 3b), similar to that in the naive group as discussed above (Supplementary Fig. 3a). (Details of the gene and peak lists are in the *source.data*)

A comparison between the RNA-seq and ATAC-seq results indicated that there was a significant overlap, as well as distinction, between the genes associated with RNA expression or chromatin accessibility changes through the hormesis regimen. This is consistent with previous findings that ATAC-seq and RNA-seq results often do not correlate[28], reflecting different modes of gene regulation that may not be correlative. The data together supported our notion that the two genomic assays together provided a more comprehensive view of the gene regulatory changes associated with our heat hormesis regimen.

Different levels of heat stress induce largely distinct RNA or chromatin accessibility changes

To further characterize the dynamic changes in RNA expression and chromatin accessibility across our hormesis regimen, we performed K-mean clustering analysis of the genes associated with significant changes in RNA-seq or ATAC-seq across the three timepoints in either the naive or primed groups and the results were visualized using heatmaps. The heatmap of 'Genes with significant RNA expression changes' includes 8,481 genes identified from RNA-seq data (Fig. 2c, Supplementary Data 1), while the heatmap of 'Genes with significant chromatin accessibility changes' includes 10,837 genes associated with 17,943 peaks identified from ATAC-seq data (Fig. 2d, Supplementary Data 2). Interestingly, despite that RNA-seq and ATAC-seq revealed substantially different genes associated with significant changes across the hormesis regimen (Supplementary Fig. 3c), the clustering analyses revealed similar pattern of changes (Fig. 2c-d). We classified these shared patterns into three categories: Priming-responsive changes (C. I), HS-responsive changes (C. II), Priming + HS-responsive changes (C. III) (Fig. 2c-d).

Priming-responsive changes (C.I) describe those exhibiting either upregulation or downregulation after priming (P1 vs NC) and showed the opposite trend following recovery (P2 vs P1). This is consistent with earlier findings that most of the priming-induced changes in RNA expression or chromatin accessibility are restored after recovery. Changes in this category were not robustly recapitulated after HS (timepoint 3) (Fig. 2c-d, Clusters (1) & (2)). The HS-responsive changes (C.II) displayed robust changes in RNA expression or chromatin accessibility upon HS (timepoint 3.3 vs timepoint 2, timepoint 3.6 vs timepoint 2), with minimal alterations observed after priming (timepoint 1) and following recovery (timepoint 2) (Fig. 2c-d, Clusters (3) & (4)). These results provided molecular evidence of dose-dependent effects, where varying levels of heat stress result in distinct molecular adaptations.

The final category (C. III) includes genes that responded to both priming and HS and most of them exhibited consistent up- or down-regulation upon priming and HS (Fig. 2c-d, Clusters (5) & (6)). Interestingly, in this category, ATAC-seq data uncovered only genes associated with significantly reduced chromatin accessibility upon priming and HS (Fig. 2d).

To understand the potential biological relevance of the various changes, we conducted Gene Ontology (GO) analyses of the various clusters. For Priming-responsive changes (C. I), we note that ribosome-related and stress response are the functional groups associated with both higher and lower expression and more and less chromatin accessibility, perhaps reflecting the dynamic nature of these classes of genes during the priming period (Fig. 2e). Similarly for HS-responsive changes (C. II), lipid metabolism and small GTPase signaling are the functional groups represented by both more and less chromatin accessibility. Interestingly, NHR transcription factors are associated with both downregulated RNA expression and less open chromatin, a class of genes likely warrant further exploration (Fig. 2f). Thus, the clustering analyses revealed that priming by mild heat stress and HS induce many distinct RNA and chromatin accessibility changes (C.I and C.II), suggesting that different levels of heat stress induce differential molecular responses, aligning with the original concept of hormesis, where a stressor generates dose-dependent effects[3,29]. For the changes that are shared between priming and HS (C.III, Priming + HS-responsive changes), mRNA processing, heat stress response, and proteolysis proteasome

were top significantly enriched functional groups associated with genes with upregulated RNA expression (848). We note that canonical heat shock response genes are among this group and their repeated induction likely contribute to the phenotypic protection confers by heat hormesis. Among genes with downregulated RNA expression (980), metabolism (lipid, short chain dehydrogenase) and detoxification stress response were top significantly enriched GO terms. Additionally, among genes with less open chromatin (567), metabolism (lipid and amino acid) was significantly enriched (Fig. 2g). The downregulation of lipid metabolism genes may reflect compensatory response to changes in membrane fluidity at the high temperature. (Details of the GO analysis can be found in the Supplementary Data 3)

Primed worms exhibit differential RNA expression and chromatin accessibility upon HS compared to naive worms

To uncover the molecular basis underlying the protective effects of primed worms, we assessed the differences in RNA expression and chromatin accessibility between primed and naive groups at the various timepoints. At timepoint 1, our finding was similar to what was discussed earlier, since naive worms did not show substantial changes, so changes between primed and naive were largely similar to those detected in primed worms comparing P1 and NC (Fig. 3a, Supplementary Fig. 3b; *source.data*). At timepoint 2, we detected only a handful of significant differences between primed and naive worms, which is consistent with our earlier conclusion that the majority of the priming-induced changes were restored after recovery (Fig. 3b; *source.data*). Our results differ from some previous studies on heat hormesis in *C. elegans*, where certain genes maintain elevated RNA expression long after the initial stress exposure has ceased[2,4,16,21]. It is important to note that our hormesis regimen is somewhat different from these studies (30°C instead of 35°C, 6 hours instead of 1 hour), and we conducted our genomic analyses using the germlineless *glp-1(ts)* mutant, making it difficult to directly compare results. Nevertheless, we found that whereas the majority of the genes induced by priming (30°C, 6 hours) restore to baseline levels

after a 12-hour recovery, a small subset of genes exhibit persistent RNA expression change (30 among 1501 upregulated, 43 among 1432 downregulated) (Supplementary Fig. 4e-f), including the HSP gene *hsp-12.3.* Some of these persistent changes could contribute to the hormetic effect. On the other hand, since most of the RNA and chromatin accessibility changes are restored after recovery, future work examining whether persistent regulation at the post-transcriptional and/or protein levels could contribute to priming induced protective effects will likely also yield informative results.

Intriguingly, despite minimal differences observed between primed and naive worms post-recovery, significant differences in both RNA expression and chromatin accessibility were detected between the two groups after HS of 3 or 6 hours (Fig. 3c, d; *source.data*). As expected, the RNA expression and chromatin accessibility differences between primed and naive worms after 3 or 6 hours of HS showed a good degree of overlap (Supplementary Fig. 4a). However, consistent with the phenotypic observation that primed worms showed greater survival advantage after a 6-hour HS compared to a 3-hour HS (Fig. 1d-e), we detected substantially more RNA expression and chromatin accessibility differences between primed and naive worms after a 6-hour HS (Fig. 3c-d). Specifically, 249 and 262 genes showed significantly up- or down-regulated RNA expression in the primed compared to the naive group (Fig. 3d). Additionally, 331 peaks (associated with 177 genes) and 123 peaks (associated with 50 genes) were significantly up- or down-regulated in the primed group (Fig. 3d). Among the genes with significantly upregulated expression (249) or more open chromatin (177) in the primed group, lipid metabolism and collagen were the significantly enriched GO term (Fig. 3e); Among the genes with significantly downregulated expression (262), detoxification stress response, pathogen stress response, and lipid metabolism were among the significantly enriched GO terms (Fig. 3f) (Supplementary Data 3).
We conducted additional clustering analysis to assess the RNA expression differences between the primed and naive groups and come to a similar conclusion that most priming-induced gene expression changes are transient, but also highlighted different waves of RNA expression differences between the primed and naive groups (Supplementray text; Supplementary Fig. 4c-d). Overall, our findings pointed to

specific differences in RNA expression and chromatin accessibility between the primed and naive groups to be likely contributors to the enhanced heat stress resilience of the primed animals.

Multiomic data unveil putative new regulators of heat hormesis

To assess whether the differential molecular changes between primed and naive worms contributed to the protective effects induced by mild heat stress priming, we selected candidate genes and tested how their RNAi knockdown might affect thermal-resistance using the regimen we described above (Fig. 1d). The first set of candidates we selected were among the ones that showed significantly upregulated RNA expression and chromatin accessibility in the primed group compared to naive after HS for 6 hours (P3.6 vs N3.6) (Fig. 3g; *source.data*). We tested five candidate genes, based on their associated GO terms, which included *endu-2*, encoding an RNA-binding protein previously reported to mediate long-term protective effects after transient heat exposure[24]. We found that RNAi knockdown of *mars-1*, but not *endu-2*, *bath-44*, *vha-9*, *cut-5*, significantly compromised the survival advantage of primed worms. Specifically, priming induced a reduced survival benefit in worms treated with *mars-1* RNAi (mean survival extension of 2.96 days) compared to those treated with an empty vector control (E.V.) (mean survival extension of 7.16 days, Fig. 3h; Supplementary Data 4). Interestingly, in naive worms, *mars-1* knockdown results in increased survival after HS compared to control (Fig. 3h). This is consistent with a known role of *mars-1* in stress response in *C. elegans*, where RNAi knockdown of *mars-1* results in enhanced oxidative stress resistance and extended lifespan in *C. elegans*[30]. *mars-1*, homologous to human *MARS1*, encodes a conserved cytoplasmic methionyl-tRNA synthetase (MetRS) that is essential for catalyzing the attachment of methionine to its cognate tRNA, a crucial step in protein synthesis. Our results suggested a link between methionine incorporation during protein synthesis and priming-induced protective effects. In human, mutations in MARS1 have been implicated in chronic activation of integrated stress response, causing peripheral nerve degeneration in familial trigeminal neuralgia patients[31], further suggesting its significant role in stress response pathways. Our results highlighted an unexpected role of MARS-1 in conferring beneficial effects in worms that have previously been primed,

as its knockdown compromises the protective effects of heat hormesis. Together, the data suggest MARS-1 plays a key and complex role in stress response, and its activity likely needs to be tuned and controlled, depending on stress levels / duration / frequency of exposure.

To better understand the transcription factors that may play a regulatory role in heat hormesis, we conducted motif analysis using significantly changed peak regions identified from ATAC-seq and the promoter regions of significantly changed genes from RNA-seq. The analysis revealed three groups of significantly enriched motifs: i) Motifs that were enriched based on both ATAC-seq and RNA-seq results; ii) Motifs enriched based on only RNA-seq or (iii) only ATAC-seq results (Table 1; *source.data*). Among the significantly enriched motifs identified based on genes showing significantly differential RNA expression and chromatin accessibility after HS, HSF-1, CEBP-1, SNPC-4, HLH-30, stood out (Table 1, pink section). HSF-1, in particular, is one of the best characterized transcription factors that is essential for mounting a heat stress response[32,33]. Interestingly, HSF-1 motif is enriched among the genes that showed upregulated RNA expression and chromatin accessibility after priming and HS, as well as those with downregulated chromatin accessibility post HS, perhaps reflecting the transient nature of some of the HSF-1 regulated gene expression[34]. CEBP-1, the homolog of C/EBP, is a conserved basic leucine zipper (bZIP) domain transcription factor with a role in stress response[35], and its motif is also enriched among genes upregulated after priming. HLH-30, the ortholog of TFEB, is a conserved basic helix-loop-helix transcription factor known for its roles in regulating stress resistance, autophagy and longevity[36], and its motif is enriched among those downregulated after priming. SNPC-4, the ortholog of SNAPC4, is a conserved small nuclear RNA activating complex, and its motif is enriched for genes with upregulated expression after HS and for peaks with greater accessibility after priming. As expected, RNAi knockdown of *hsf-1* completely abolished the enhanced survival to HS of the primed worms (Fig. 4a). Intriguingly, knocking down *snpc-4* also significantly compromised the survival advantage induced by priming using our heat hormesis regimen (Fig. 4b). However, no effects were detected with knockdowns of *cebp-1* and *hlh-30* under our hormesis regimen (Supplementary Data 4).

SNPC-4, a subunit of the small nuclear RNA (snRNA)-activating protein complex (SNAPc), is essential in regulating piRNA transcription in *C. elegans*[37,38]. SNAPc is known for its role in mediating trans-splicing as survival strategy during food deprivation in worms. In human, SNAPC4 variants are linked to neural and developmental disorders due to the dysregulation of alternative splicing[39,40]. These studies suggest that SNPC-4 could be a pivotal player in stress response adaptation via post-transcriptional mechanisms. Although direct evidence connecting SNPC-4 to heat stress has not been established, previous studies indicate that high temperatures may inhibit piRNA biogenesis, leading to transcriptional changes essential for stress adaptation[41]. Intriguingly, we found that *prg-1*, which encodes a Piwi-family Argonaute protein that interacts with 21U-RNAs (piRNAs)[42], is persistently upregulated after priming, recovery, and a 3-hour HS, bolstering the hypothesis of SNPC-4's involvement in heat hormesis through piRNA regulation. Together, these findings provide exciting connections, and further support our hypothesis that SNPC-4 modulates the piRNA pathway to contribute to stress adaptation in heat hormesis.

The motifs revealed by differential RNA-seq data included three GATA transcription factors, ELT-2, ELT-3, ELT-6, and a zinc finger transcription factor, PQM-1 (Table 1, green section; *source.data*). All four motifs were enriched among genes that showed downregulation after both priming and HS in the primed compared to naive groups. A recent study showed that the ELT-2 motif is enriched in genes upregulated in *hsf-1(sy441)* mutant and *hsf-1*(RNAi) worms. PQM-1 is known to work antagonistically with DAF-16 in regulating stress responses within the DAF-2 pathway[43]. Excitingly, our results showed that RNAi knockdown of *elt-2* completely abolished the heat shock survival advantage in primed worms (Fig. 4c). However, knockdowns of *elt-6* and *pqm-1* did not compromise the survival benefits conferred by priming using our hormesis regimen (Supplementary Data 4).

ELT-2, the *C. elegans* ortholog of human GATA4, GATA5 and GATA6, plays a predominant role in regulating intestinal development, innate immunity, and multi-pathogen responses[44–46]. Intriguingly, Kovács et al.[22] showed that ELT-2 is essential for the increased thermal-tolerance observed in HSF-1-deficient worms, linking heat stress resistance to innate immunity-related signaling pathways. Our

findings extend this link by demonstrating ELT-2's involvement in heat hormesis, providing a new perspective on its functional role. It will be interesting to further explore whether ELT-2 and HSF-1 act through common or independent molecular pathways in mediating heat hormesis, potentially unveiling mechanistic understanding between stress response mechanisms and developmental signaling.

Several motifs were revealed based on differential ATAC-seq data (Table 1, blue section; *source.data*). Specifically, DPY-27, a homolog of the chromosome condensation protein essential for dosage compensation[47], has its motif highly enriched in peaks downregulated after both priming and HS in the primed compared to naive groups. EOR-1, the homolog of the Promyelocytic Leukemia Zinc Finger (PLZF) factor, implicated in regulating chromatin dynamic during development[48,49], has its motif enriched in peaks upregulated after both priming and HS. Additionally, FOS-1 and ATF-7 motifs are enriched among peaks upregulated after HS. FOS-1 and ATF-7, both conserved bZIP transcription factors, have been implicated in the regulation of stress responses and longevity[50,51]. We observed that while RNAi knockdown of *fos-1* and *dpy-27* consistently compromised the heat survival advantage of primed worms in multiple replicates, the results did not reach statistical significance (Supplementary 5a-b; Supplementary Data 4). We note that variability in survival time between experiments, potentially influenced by environmental factors other than temperature, or RNAi efficiency, may contribute to these fluctuations. In contrast, knockdown of *atf-7* did not impact the priming-induced survival extension phenotypes (Supplementary Data 4). We therefore interpreted the results to suggest that *fos-1* and *dpy-27* might also play a role in enhancing thermal resistance through priming.

FOS-1/c-Fos is a component of the highly conserved activator protein-1 (AP-1) complex, which is known to regulate diverse functions including cell cycle progression, cell death, development, immunity, and stress response in vertebrates[52]. In *C. elegans*, FOS-1 regulates hyperosmotic stress and acts as a downstream transcriptional activator of the highly conserve stress-activated JNK protein kinase pathway[50,53]. Moreover, a recent study presents compelling evidence that, with aging, mammalian AP-1 progressively shifts its occupancy from chromatin sites linked to cell identity and development to those

involved in stimuli and stress response, resulting in remodeling of chromatin accessibility due to its pioneer transcription factor activity[54,55]. The age-dependent AP1 redistribution on the chromatin was speculated to reflect either the natural progression of transcriptional reprogramming as cells and organisms mature and age, or the incomplete reversal of AP1 (and other transcription factors) occupancy after stimuli or stress responses, thus representing a type of "epigenetic memory". The latter hypothesis may align with our findings, where FOS-1 DNA motif is specifically enriched in more open chromatin regions in primed worms upon HS re-challenge, suggesting its role in maintaining stress memory through chromatin opening in heat hormesis.

DPY-27, a homolog of human SMC4, is a subunit of the dosage compensation complex (DCC), resembling condensin, and is essential for controlling chromosome structure and resolution during cell division across species from yeast to humans. In *C. elegans*, the DCC binds to both X chromosomes, where it reduces transcription by half primarily through decreased recruitment of RNA polymerase II, thus balancing X chromosome expression[47]. The DCC is recruited to the X chromosome to form topologically associated domain (TAD) boundaries that regulate chromosome-wide gene expression. Intriguingly, recent studies have shown that eliminating DCC-dependent TADs on the X chromosome reduces worms' tolerance to heat and shortens lifespan, without affecting dosage compensation-related gene expression during embryogenesis[56,57]. This suggests a role for chromosome architecture regulated by the DCC in modulating stress responses and aging. In our study, DPY-27's motif was markedly enriched in less accessible chromatin regions following both priming and heat shock, further linking DCC-mediated chromosome architecture regulation to heat hormesis.

Together, these findings identify HSF-1, SNPC-4, ELT-2, and potentially FOS-1 and DPY-27, as critical mediators of the thermal-resistance phenotype induced by our heat hormesis regimen. Their further characterization promises to uncover fundamental molecular mechanisms governing heat hormesis and could pave the way for novel health-promoting therapuetics. Moreover, this study provides a powerful proof-of-principle for leveraging multiomic analyses in combination with functional assays to decode

conserved principles of complex biological phenomemnon. Importantly, our comprehensive genomic dataset represents a valuable resource for future investigations, opening new avenues for research into stress resilience and therapeutic innovation.

Resource Availability

Lead contact

Requests for further information and resources should be directed to and will be fulfilled by the lead contact, Siu Sylvia Lee (sylvia.lee@cornell.edu)

Data and code availability

ATAC-seq and RNA-seq raw sequencing data, ATAC-seq BedGraph files for visualization, the RNA-seq raw read count matrix, and the ATAC-seq raw read count matrix for identified 'consensus peaks' are in the process of being deposited in NCBI's Gene Expression Omnibus (GEO) and will be accessible upon request or before the final submission. Details on reference files used for genome alignment (ce11/WBcel235) and other analyses are provided in the STAR Methods section. Raw data for all thermal-resistance, survival, and lifespan experiments; gene lists; peak (associated gene) lists; BED format files of consensus peaks; motif candidate lists; and other data corresponding to the main and supplementary figures can be found in *source.data*. RNAi screening results, gene lists and peak (associated gene) lists in heatmaps from K-means clustering, and GO enrichment lists are available in the Supplementary Information (additional Summplementary files). All custom computer codes used for analyses in this study are available in the Supplementary Information (Supplementary Data 5-10).

Acknowledgements

Thank you to the Lee Lab members for discussions and suggestions on experimental design and data analysis, and to the lab technicians for support with supplies and preparations. Thank you to the Cornell Genomics Innovation Hub/TREx (Dr. Adrian McNairn) for ATAC-seq advice and to Faraz Ahmed and Dr. Paul Munn for guidance on the analysis pipeline. Thank you to the Cornell Institute of Biotechnology for Illumina sequencing and quality control, with specific appreciation to Dr. Qi Sun and Dr. Jeff Glaubitz for bioinformatics consultation. Thank you to the Cornell Statistical Consulting Unit for statistical advice. Strains were provided by the Caenorhabditis Genetics Center (CGC), and Wormbase.org was used throughout this study[58]. This work was funded by NIH AG024425 (to S.S.L.), the Taiwanese Study Abroad Scholarship from Ministry of Education Taiwan (to H.-Y.C.), and the Genomics Innovation Seed Grant from Cornell Institute of Biotechnology.

Author contributions

H.-Y.C. and S.S.L. designed the study and wrote the paper. S.M. and S.M. conducted partial RNA-seq and ATAC-seq data analyses. C.M. and S.S. carried out some of the thermal-resistance and RNAi experiments. C.G.D. supervised the analysis pipelines. H.-Y.C. conducted all other experiments and data analyses. S.S.L. secured funding and supervised the experimental plans.

Declaration of interests

The authors declare no competing interests.

Declaration of generative AI and AI-assisted technologies

During the preparation of this work the authors used ChatGPT-4o in order to improve language and readibility. After using this tool/service, the authors reviewed and edited the content as needed and take full responsibility for the content of the publication.

Supplementary Information

Supplementary Information document: Supplementary text, Supplementary Figures 1-5, and Descrptions of additional supplementary files.

Thirteen additional supplementary files (Supplementary Data 1-13) is provided.

Methods

C. elegans maintenance

Unless otherwise specified, worms were maintained on 6-cm NGM plates seeded with 0.2 ml of a five-times concentrated overnight culture of streptomycin-resistant OP50 bacteria (live OP50). Killed OP50 bacteria were prepared by resuspending live OP50 in LB containing 100µg/ml Carbenicillin and 15µg/ml Tetracycline twice, then concentrating it twentyfold. The bacteria incubated with the antibiotic on a rocker for at least 30 minutes before use. Killed OP50 was used to mitigate bacterial infections in *glp-1 (ts)* mutant strains (*e2141* temperature sensitive allele) during survival assays. The N2 strain was typically kept at 20°C, while the *glp-1 (ts)* mutant strain was maintained at 16°C unless noted differently.

Growth of synchronized worms on a small scale for phenotypic experiments

For the wildtype N2 strain: Several plates were set up with 4-5 gravid adults per plate for egg laying at 20°C for 3-4 hours. After egg laying, the gravid adults were removed, and the eggs were incubated at 20°C for approximately 65 hours. The synchronized gravid adults were then distributed to fresh plates, approximately 30 per plate before the experiments began. Priming was performed at this time when the N2 worms just reached gravid adults of their Day1 (D1) adult stage. **For the *glp-1(ts)* mutant strain:** Several plates were set up with 6-8 gravid adults per plate for egg laying at 16°C for 4-5 hours. The gravid adults were removed after egg laying, and the eggs were incubated at 25°C for approximately 48

hours until they became young adults and were transferred to 20°C ("Young adult" refers to the developmental stage immediately after the L4 stage, in which the worm has molted into a reproductive adult but has not yet begun laying a large number of eggs). After incubating overnight at 20°C (approximately 15-17 hours), the synchronized adults were distributed to fresh plates with Killed OP50, approximately 30 per plate, before starting experiments. Priming was performed at this time when sterile *glp-1(ts)* worms were approximately at their D2 adult stage. The wildtype N2 was sometimes conducted in parallel as a positive control, following the same maintenance protocol as *glp-1(ts)*.

Priming and Heat shock (HS) experimental setup

Worms were subjected to incubators with setting pre-adjusted to target temperatures (30°C for 6 hours for priming, and specific temperatures and duration for HS depending on the experiment). During incubation, the lids of the plates were replaced with those having manually drilled holes, and the plates were wrapped with parafilm on the sides. The plates were placed on a metal rack in the incubator with agar side facing down. This setup aimed to allow worms to reach the target temperature more efficiently and to maintain consistent temperature and humidity inside the plates. After temperature treatments, the parafilm was removed, and the lids were switched back to the normal ones without holes before being moved back to 20°C.

Thermal-resistance assay

To explore how priming affected thermal resistance, defined as regaining motility after exposure to the indicated HS temperature and duration, we conducted tests. For small-scale phenotypic experiments, 30-40 worms were placed on each 6-cm plate, with at least two plates per group for each biological replicate. For large-scale experiments, approximately 1000 worms were placed on each 10-cm plate. After being subjected to HS at 35°C for 10 hours or other specified temperatures and durations detailed in the

source.data, worms were maintained at 20°C until scoring. Scoring occurred 15 hours post-HS, with each plate being tapped 10 times consistently immediately before scoring. For small-scale experiments, worms that moved without being touched by a picker were counted, along with the total number of worms, to calculate the percentage of moving worms. For large-scale experiments, a consistently marked 1/9 area of each 10 cm plate was used to count worms that moved without being touched and the total worms within the marked area to calculate the percentage of moving worms. Three separate areas were marked and scored for each experimental group as technical replicates. Three independent experiments were conducted as biological replicates. The average percentage of moving and standard deviation (std) were calculated. 2-tailed unequal variances t-test was performed to determine if the differences between primed and naive groups were significant.

Survival assay after HS

Synchronized worms were subjected to priming, recovery, and HS or were maintained without priming for the naive group, according to specific temperatures and durations as detailed in *source.data*. After HS, worms were scored every two days until all had died. Worms were scored as dead when they failed to respond to a gentle prod on the head by a worm picker. Worms were maintained at 20°C after HS and throughout the experiments. Data were analyzed using OASIS2 online survival analysis tool[59]. The Kaplan-Meier estimator was used to re-plot survival curves in Excel, with the 'Fraction alive' on the y-axis and days after HS on the x-axis. Log-rank tests were utilized to determine if there were significant differences in survival times between the two groups. All survival assay experiments were conducted independently at least twice. (See *source.data* for raw data and analysis details)

Lifespan

Synchronized worms were subjected to priming, or were maintained without priming for the naive group, at the indicated timing mentioned above and detailed in *source.data*. Worms were scored subsequently every two days until all had died. Worms were scored as dead when they failed to respond to a gentle prod on the head by a worm picker. For the wildtype N2 strain, worms were transferred to fresh plates every 1-2 days until the end of their reproductive period. The chemical 5-fluoro-2'-deoxyuridine (FUDR) was not used. For *glp-1(ts)* mutant strain, worms for both primed and naive groups were transferred to plates with Killed OP50 before the priming experiments. Data were analyzed using OASIS2 online survival analysis tool as mentioned above. The Kaplan-Meier estimator was used to re-plot survival curves in Excel, with the 'Fraction alive' on the y-axis and days after HS on the x-axis. Log-rank tests were utilized to determine if there were significant differences in survival times between the two groups. All lifespan assay experiments were conducted independently at least twice. (See *source.data* for raw data and analysis details)

Reproductive function experiments

Wildtype N2 worms were maintained, synchronized at 20°C. After approximately 65 hours of development from eggs, newly matured gravid adults were distributed, one per 3.5 cm plate. The primed group was subjected to a 6-hour priming at 30°C and returned to 20°C, while Naive group was maintained at 20°C in parallel during priming period. After priming, each worm was transferred to a new 3.5 cm plate to continue laying eggs, and the eggs left on the original plate were counted. The worms were subsequently transferred to new plates every 12 hours until they stopped laying eggs (~5days). Once counted, the eggs were incubated at 20°C to allow for hatching. Larvae were then counted 24 hours later. In total, 9 data points for both egg and larvae counts were collected. The average total broodsize was calculated by summing egg counts from 9-timepoints across the reproductive period of 25 individual

single worms. The average broodsize for each time frame (6 hours for the first timepoint and 12 hours for the subsequent eight timepoints) was calculated across these 25 worms. The average hatching rate for each timepoints was calculated by dividing the number of eggs by the number of larvae for 25 worms. Hatching rates were adjusted to 1 if the values exceeded 1 to account for potential miscounts of eggs, which might be less visible than larvae during counting. Data of 25 worms were collected across three independent experiments, with each biological replicate containing around 5~10 worms per group. (Details in *source.data)*

RNA interference

HT115 bacteria expressing double-stranded RNA against the gene of interest were obtained from the Ahringer[60] or Vidal[61] libraries and verified by Sanger sequencing. RNAi bacteria and the control empty vector (E.V.), L4440, were cultured overnight in LB containing 100 µg/ml carbenicillin and shaken at 37°C for 3-4 hours until an optical density of 0.6-0.8 was reached. The cultures were then induced with 1mM of IPTG and continued to incubate on a shaker at 37°C for an additional 2.5 hours. After induction, the bacteria were centrifuged at 2000 rpm for 15 minutes at room temperature and concentrated 50-fold. 200µl of concentrated bacteria were seeded on 6-cm 'RNAi plates", which are NGM plates modified by omitting streptomycin and adding 100 µg/ml ampicillin, 15 µg/ml tetracycline, and 1mM IPTG. RNAi was administered to worms through feeding. The timing of RNAi administration varied depending on the genes, considering any developmental phenotypes caused by knocking down the gene. Details of the RNAi administration timing for each gene are documented in the Supplementary Data 4. To determine whether RNAi knockdown of a specific gene compromises the priming-induced phenotype in survival extension, the survival extension rate is calculated using the formula: *(Mean survival days in primed−Mean survival days in* Naïve*)/Mean survival days in naïve * 100*. This measure quantifies the increase in mean survival days in primed group relative to naïve group in each independent experiment.

To statistically evaluate whether the survival extension is significantly reduced upon gene silencing, a paired two-tailed t-test is employed.

Collection of timed samples synchronized worms on a large scale for sequencing

For *glp-1*(ts) mutant strain, five gravid adults were grown on several 6-cm NGM plates containing 0.2ml of a five-times concentrated overnight culture of streptomycin-resistant OP50 for 6 days at 16°C until the plates were full of mixture stages of worms and embryos without running out of the OP50. 1ml M9 buffer with 0.05% TWEEN20 was added into each 6-cm plate without disturbing the bacteria lawn to avoid collecting embryos. (TWEEN20 was used to avoid worms sticking on the tips during the process) M9 buffer with 0.05%TWEEN20 containing adults and larvae was then collected into centrifuge tubes. The supernatant containing larvae was removed around 30-60 sec while most of the adults settled down to the bottom of the tube. Using this strategy to separate adults and larvae by washing worms several times until the tube mostly contained adults. Fully resuspended adults in 1 ml M9 buffer with 0.05% TWEEN20 and aliquot 10 µl out to count the number of adults. Based on the counting numbers, proportionally distributed the desired amount of the adults to new plates for egg laying.

10-cm NGM plates containing 1ml of a 25-times concentrated overnight culture of streptomycin-resistant OP50 were used for growing larger amounts of worms. 1000-2000 adults were placed on 10-cm plates and incubated at 16°C for 4-5 hours for egg laying. 5ml M9 buffer was applied to wash off adult worms from the plates without disturbing the bacteria lawn. Repeated the washing step until most of the adults were removed. 5ml m9 with 0.05%TWEEN20 was applied to wash off the bacterial lawn containing embryos using the liquid force generated by several pipetting. The liquid containing embryos were then collected into centrifuge tubes and were spun down in a centrifuge for one minute at 2000 rpm. Removed the supernatant and resuspended the pelleted embryos thoroughly in My with 0.05% TWEEN20. The number of synchronized embryos was quantified by proportionally counting and around 1200 embryos

were distributed per 10-cm plates. At the assigned timepoints, synchronized worms were washed off and collected into centrifuge tubes using M9 with 0.05% TWEEN20. After the worms settled in the bottom of the tubes, removed supernatant and transferred worms to 1.7ml low-binding tubes. Worms were washed by M9 buffer several (1-5) times until the supernatant was clear indicating most of the bacteria was removed. 200 worms were then aliquoted to another low-binding tube and snap-frozen in 1ml TRIZOL after removing most of the M9 buffer in liquid nitrogen for RNA-seq. The remaining 1000 worms were snap-frozen after removing most of the M9 buffer in liquid nitrogen for ATAC-seq. After snap frozen, all samples were stored at -80°C until further processing.

Five biological replicates for RNA-seq (labeled R_r1, R_r2, R_r3, R_r4, R_r5) and four for ATAC-seq (labeled A_r1, A_r2, A_r3, A_r4) were processed in two independent sequencing batches. For RNA-seq, R_r1, R_r2, and R_r3 were in the first batch, and R_r4 and R_r5 in the second. For ATAC-seq, A_r1 and A_r2 were in the first batch, and A_r3 and A_r4 in the second. Each replicate includes samples from multiple timepoints across our regimen in both primed and naive groups (Fig. 1a). Data from all timepoints have at least three biological replicates, except for T3.6, which has two biological replicates in ATAC-seq.

RNA extraction and RNA-seq

200 worms per sample were snap-frozen in 1 ml of TRIzol, as previously described, and homogenized by alternating between thawing, vortexing, and refreezing in liquid nitrogen four times. 200 µl of chloroform was added to each tube, samples were vortexed for 15 seconds, incubated at room temperature for 3 minutes, and then centrifuged at 12,000 g for 15 minutes at 4°C. The upper aqueous layer was transferred to a fresh tube, and 500 µl of isopropanol was added to each sample. After adding 1 µl of GlycoBlue and incubating for 15 minutes at room temperature, samples were centrifuged at 12,000 g for 10 minutes at 4°C. The supernatant was discarded, and the RNA pellet was washed with 1 ml of 80% ethanol. All remaining ethanol was removed after centrifugation at 12,000 g for 10 minutes at 4°C, and the RNA

pellet was air-dried for 5-7 minutes and then dissolved in 17 µl of DEPC water. The RNA was then treated with DNase to remove residual DNA, following the instructions from the TURBO DNase kit (Invitrogen AM1907). After DNase treatment, the RNA was further purified using an RNA cleanup kit (ZYMO Research R1015). RNA concentration was measured using the Qubit RNA HS Assay kit (ThermoFisher Q32851). Five biological replicates were processed as described above.

RNA-seq libraries were prepared using the QuantSeq 3' mRNA-Seq Library Prep Kit (Lexogen FWD 015). For replicates R_r1, R_r2, and R_r3, the preparation started with 100 ng of RNA from each sample and employing 15 PCR cycles. For replicates R_r4 and R_r5, the libraries were prepared starting with 70 ng of RNA and employing 17 PCR cycles. The libraries were quantified using a Qubit DNA HS Assay kit and their quality was assessed with a Bioanalyzer. Subsequently, the libraries were submitted for single-end 86 bp sequencing on an Illumina NextSeq 500 machine. Replicates R_r1, R_r2, and R_r3 were pooled in one sequencing lane, while R_r4 and R_r5 were pooled in another, with each pool sequenced in separate runs.

RNA-seq data analysis

Upstream analysis:

Adaptor sequences were trimmed, and low-quality reads filtered from raw fastq files using the trim_galore function in Cutadapt (version 4.6) with settings -q 20 --fastqc. Trimmed sequencing reads from the FASTQ files were then aligned to the reference genome (ce11/WBcel235) using STAR aligner. Initially, the reference genome was indexed with the following settings: --runThreadN 8 --runMode genomeGenerate --genomeDir [genome_directory] --genomeFastaFiles [genome fasta_file] --sjdbGTFfile [gtf_file] --sjdbOverhang [read length – 1]. Alignment was performed using STAR settings: --quantMode GeneCounts --genomeDir [genome_directory] --readFilesIn [trimmed sequencing file] --readFilesCommand zcat --runThreadN 2 --outFileNamePrefix [output_file_prefix] --

outFilterMultimapNmax 1 --outFilterMismatchNmax 2 --outSAMtype BAM SortedByCoordinate. The resulting tab-delimited text files, named with the prefix "_ReadsPerGene.out.tab", contained counts for reads aligned to the plus strand of RNA in column 3, which is recommended and applied for 3' RNA-seq data. Counts from each sample were aggregated to generate a matrix that was uploaded to RStudio for downstream differential gene expression analysis (Supplementary Data 6).

Total aligned reads and the percentage of uniquely mapped reads from all sequencing files were accessed. Only uniquely mapped reads were utilized for downstream analysis (*source.data*: RNA-seq QC). The correlation of aligned reads across biological replicates was calculated using Spearman correlation and visualized with a heatmap using Morpheus (https://software.broadinstitute.org/morpheus). (Supplementary Fig. 2a-e). The color scheme of the heatmap displays a minimum value of 0.85 and a maximum value of 1.

Differential RNA expression analysis:

A matrix (Supplementary Data 11) containing raw read counts was generated and uploaded to RStudio for DESeq2 analysis. The matrix was subsetted according to timepoints and replicates for further comparison. For comparisons involving timepoints 1, 2, and 3.3, columns including five replicates (R_r1, R_r2, R_r3, R_r4, and R_r5) for samples (NC, N1, P1, N2, P2, N3.3, and P3.3) were subsetted. For comparisons involving timepoint 3.6, columns including three replicates (R_r1, R_r2, and R_r3) for samples (NC, N1, P1, N2, P2, N3.3, P3.3, N3.6, and P3.6) were used. Prior to differential analysis, read counts were normalized using the estimateSizeFactors function. The normalized counts were then filtered to retain only genes with more than 5 normalized counts in at least the minimum number of replicates per sample. To better estimate log2 Fold Change (log2FC) for genes with low counts and high dispersion, the apeglm method was employed for shrinkage during differential analysis. Genes with adjusted p-values less than

0.05 were considered significant. MA plots were generated using methods described in the ATAC-seq analysis section (Supplementary Data 7)

Nuclei purification and ATAC-seq

Worms, previously snap-frozen and stored in low-binding tubes, were thawed on ice. All subsequent steps were conducted on ice or at 4°C, with all materials pre-chilled to maintain nuclei integrity. An equal volume of freshly prepared Nuclei Purification Buffer (NPB)[48] (recipe available in *source.data: ATAC protocol*) was added to the worm pellet. The worms were homogenized manually five times using Pellet Pestles coated with Fetal Bovine Serum. The homogenization frequency was optimized to minimize damaging nuclei. After homogenization, worm pellets were allowed to settle for 3-5 minutes, then centrifuged at 100-200 g for 3 minutes. The supernatant, containing the nuclei, was transferred to a fresh low-binding tube. The remaining worm pellets were resuspended in an equal volume of 2X NPB and homogenized again as described. This process was repeated for multiple rounds until no visible worm pellet remained, typically requiring 7-8 rounds. The first six rounds involved homogenizing five times, with the final rounds reduced to three times to preserve nuclei integrity. After completing the homogenization, the collected supernatants were centrifuged at 100-200 g to remove debris, transferring the clean supernatant into a new tube. A subset of nuclei was stained with DAPI and examined under a fluorescence microscope to assess quality. Nuclei counts were determined using a hemocytometer with DAPI staining. For ATAC-seq, 50,000 nuclei per sample were aliquoted into a standard tube (non-low-binding) and pelleted by centrifugation at 1,000 g for 10 minutes. The pellet location was marked, and the supernatant was carefully removed to avoid contamination with bacterial DNA.

Purified nuclei were immediately subjected to the ATAC-seq procedure. Nuclei were gently resuspended in 47.5 µl Omni-ATAC buffer (composed of 2X Illumina Tagment DNA (TD) buffer, 16.5 µl 1X PBS, 0.1% TWEEN20, and 0.01% Digitonin) and mixed with 2.5µl of Illumina Tagment DNA Enzyme

(TDE1) (Cat#20034197). The mixture was incubated at 37°C on a thermomixer set to 500 rpm for 0.5-1 hour. Tagmented DNA was then purified using a MinElute PCR Purification Kit (Qiagen #28004) and eluted in 10µl. The purified DNA fragments were stored at -20°C until PCR amplification (Details in *source.data*: ATAC protocol).

PCR amplification was performed using NEBNext Ultra II Q5 Master Mix (M0544S) in a total volume of 50 µl, with 9 µl of purified tagmented DNA and 25 µM primer concentration. The thermocycling protocol included an initial step at 72°C for 5 minutes, followed by 98°C for 30 seconds, and 12 cycles of 98°C for 10 seconds, 63°C for 30 seconds, and 72°C for 1 minute. Each sample utilized a common Adapter 1 primer (Ad1) and a unique index Adapter 2 (Ad2*) primer (Details in the *source.data*: ATAC protocol).

Amplified ATAC-seq DNA libraries were purified using the MinElute PCR Purification Kit (Qiagen #28004) and eluted in 25µl of warm DEPC water. Libraries were size-selected to retain DNA fragments between 100bp-600bp using Blue Pippin service, quantified using a Qubit, and quality-checked using a Bioanalyzer. Sequencing was performed on an Illumina NextSeq 500 machine, with libraries from replicates A_r1 and A_r2 pooled at a final concentration of 3.6 ng/µl for one sequencing lane, and libraries from replicates A_r3 and A_r4 pooled at a concentration of 1.96 ng/µl for another lane. Each pool was sequenced independently.

ATAC-seq data analysis

Upstream analysis: From Raw data to final BAM files:

FASTQ files were downloaded using the command wget -q -c -O. The paired-end FASTQ files, denoted as .R1 and .R2, were organized for processing. Adapters were trimmed using Cutadapt (version 4.6) integrated with Trim Galore, applying the parameters --gzip -nextseq 20 --cores 8 --paired. The trimmed,

paired-end sequencing files were then aligned to the reference genome Caenorhabditis elegans WBcel235 (ce11) using BWA with settings -t 8 -M. Following alignment, SAM files were converted to BAM format and subsequently sorted and indexed using SAMtools. To refine the BAM files further, mitochondrial DNA sequences were excluded using samtools view. Sequences listed in the Caenorhabditis elegans ce11 blacklist (version 2) were also removed using bedtools intersect. Duplicate reads were marked using Picard Tools' MarkDuplicates and excluded with samtools view -F 0X400. The resultant BAM files, purged of mitochondrial DNA, blacklist regions, and duplicates, were indexed for downstream analysis.

Quality control (QC) and Transcription Start Site (TSS) enrichment analysis:

Quality control metrics were assessed using several tools. Aligned and uniquely mapped reads were quantified using samtools view -c, while samtools idxstats provided percentages of mitochondrial DNA (mtDNA) reads. Duplicate read percentages were determined using Picard Tools' MarkDuplicates function and summarized in MultiQC reports (*source.data*: ATAC-seq QC). For TSS enrichment analysis, the DeepTools suite was utilized. BAM files were first converted to BigWig format with bamCoverage, which translates raw read counts into coverage tracks. This step was performed without scaling adjustments to preserve original read densities. TSS signal coverage was then calculated for regions spanning 1000 bp upstream and downstream of each TSS using the computeMatrix command (settings: reference-point -a 1000 -b 1000). Heatmaps visualizing these coverage intensities were generated with plotHeatmap. All samples demonstrated enriched reads at TSS, aligning with a distinct peak at each TSS. The reference TSS data, adopted from Chen et al.[62], was based on transcription initiation cluster (TIC) ‘mode positions’ mapped to the ce10/WS220 genome. To ensure compatibility with our analyses, which utilized the ce11 reference genome, TSS data was converted using the UCSC LiftOver Tool

Peak calling:

Following quality control of the upstream analysis, final indexed BAM files were utilized for narrow peak calling. Each sample and replicate underwent peak calling independently using MACS2 (version 2.2.7.1-r9). The settings employed were -f BAMPE --bdg --SPMR --gsize ce -q 0.05 --call-summits, with the default local correction parameters set to --slocal 1000 --llocal 10000. For visualization of read coverages, the makeTagDirectory function from the Homer software suite was used to create tag.dir. Bedgraph files were then generated using the makeUCSfile function with the parameters .tag.dir -o auto -fsize 1e10 -res 1 -color 106,42,73 -style chipseq.

Identifying 'consensus peaks' and quantification of reads in peaks:

To identify 'consensus peaks' for differential chromatin accessibility analysis, a three-step process was implemented:

1. **Merging read files:** BAM files from all biological replicates within each experimental group were merged using the samtools merge command. Experimental groups included NC, N1, N2, N3.3, P1, P2, P3.3 with four biological replicates each, and N3.6, P3.6 with two biological replicates each.
2. **Calling consensus peaks:** Using MACS2, consensus narrow peaks were called from a single command line that included all merged BAM files as inputs, using settings previously described.
3. **Subdividing peaks based on summits:** The identified consensus narrow peaks were further subdivided based on their summits using the splitMACS2SubPeaks.perl script (adapted from Daugherty et al.[48]. This subdivision produced a total of 30,404 'Consensus Peaks' with an average length of 481 bp. Details of the genomic region for the 30,404 Consensus Peaks, labeled with the PeakID syntax '4reps.HS6hr_ConsensusPeaks_peak_', are available in *source.data: 30,404 Consensus* Peaks.

Quantification of reads in peaks: Reads within these 'consensus peaks' for each individual sample were quantified using the featureCounts program, facilitating subsequent analyses of chromatin accessibility variations across samples.

QC and consistency of biological replicates:

FRiP scores, representing the fraction of mapped reads in identified region of consensus peaks, were calculated for each sample using the featureCounts program and aggregated with multiqc. Across all samples, FRiP scores ranged from 31% to 49%, indicating no significant variance among biological replicates and suggesting reliable peak calling and reproducibility across different batches (Supplementary Fig. 2k). To further assess the consistency of biological replicates, genome-wide correlations of mapped reads between biological replicates were analyzed using the bedtools multicov function with a 2 kb sliding window across the ce11genome, segmented by the bedtools makewindows function. Read counts from each BAM file in each 2 kb window were logged (log10 transformation) and uploaded into RStudio. Pearson's correlation coefficients between each replicate were calculated using the cor function in R, compiled into a matrix, and visualized using the heatmap.2 function from the gplots package in R, categorizing samples by timepoints for clarity in correlation assessment (Supplementary Fig. 2f-j).
(Supplementary Data 5)

Differential analysis of chromatin accessibility:

A matrix containing raw read counts in consensus peaks was generated and uploaded to RStudio for DESeq2 analysis. The matrix encompassed four biological replicates (A-r1, A-r2, A-r3, A-r4) for samples: NC, N1, P1, N2, P2, N3.3, and P3.3 and two biological replicates (A-r1, A-r2) for the samples:

N3.6 and P3.6. (Supplementary Data 12). This matrix was loaded into RStudio and served as input for DESeq2 for differential analysis. Prior to analysis, read counts were normalized using the estimateSizeFactors function. Only peaks with more than five normalized counts in at least two samples, the minimum number of replicates in some experimental groups, were retained for analysis. To refine the estimation of log2 Fold Change (log2FC) for peaks with low counts and high dispersion, the apeglm method was utilized for shrinkage during the differential analysis. Peaks with adjusted p-values below 0.05 were determined significant. MA plots were generated via ggplot2, where peaks significantly upregulated are marked in red and those downregulated in blue. Additionally, peaks upregulated after priming but downregulated after recovery were highlighted in pink (P1 vs NC up, P2 vs P1 down), and those downregulated after priming but upregulated after recovery were marked in light blue (P1 vs NC down, P2 vs P1 up), assigning additional categories and colors in the plots for clearer visualization and interpretation (Supplementary Data 7).

Peak annotation:

For annotating consensus peaks, a dataset of 42,245 accessible elements, termed Reference Elements, derived from the study by Jänes et al.[63] (elife-37344-fig1-data1-v2) was utilized. These Reference Elements, adapted using ce11 genome information (Supplementary Data 13), facilitated the annotation of consensus peaks, which involved matching consensus peaks to Reference Elements with at least a 50% overlap. This annotation process was conducted using the 'findOverlapsOfPeaks' function within the 'ChIPpeakAnno' R package (Supplementary Data 8). A total of 30,404 consensus peaks were annotated, linking them to 19,352 functional information records that included associated genes and functional elements such as promoters and enhancers (*source.data: annotated.ConsensusPeaks*).

Motif analysis

Motif enrichment analysis was performed using the Simple Enrichment Analysis (SEA) tool from THE MEME Suite (version 5.5.7)[64]. To identify motifs enriched in the promoter regions of significant genes from RNA-seq data, promoter sequences were obtained from the regions either 500bp or 2000bp upstream of the TSS following 'Supplementary Data 9'. The input sequences comprised promoter sequences from significant genes, while control sequences were promoter sequences from non-significant genes. For motif enriched in significant peak regions from ATAC-seq data, BED files composed of significant peak regions were used as input sequences, while non-significant peak regions were used as control sequences.

The 'JASPARA (non-redundant)-nematode2022[65]' and 'CIS-BP 2.0 Single Species-Caenorhabditis_elegans[66]' motif databases were applied to identify motif enrichments. Enrichment was considered significant if the Q-value was less than 0.05. Significantly enriched motifs were selected as candidates for RNAi screening if their associated genes showed detectable expression levels in our RNA-seq data. We primarily selected motif candidates identified in the JASPARA database for our RNAi screening, as the database has undergone more functional validation compared to the motifs in CIS-BP. Similar motifs were detected in both databases, while the hsf-1 motif was found exclusively in CIS-BP and not in JASPAR. (Motif list can be found in *source.data*)

Temporal dynamic analysis and trajectory plotting

For the temporal dynamic analysis, data input of genes with their Log2FC between prime and naive groups across timepoints were loaded into R script (Supplementary Data 10). Clustering was performed using the K-means algorithm (dtwclust), grouping genes into eight clusters based on similar temporal dynamic patterns. Euclidean distance was used in clustering to highlight shared trends over time. Mean expression profiles for each cluster were calculated and visualized using ggplot2 to display cluster-

specific temporal patterns. Additionally, individual cluster plots were generated using highcharter to provide a dynamic view of each gene's temporal trajectory within each cluster. The code is openly available on our GitHub repository at https://github.com/Rathalodusk/TimeSeriesClus.

Statistical information

Statistical analyses for thermal-tolerance and reproductive function experiments were performed using Microsoft Excel or GraphPad. Lifespan and survival assays after heat shock were analyzed using OASIS 2[59]. Gene ontology analysis utilized WormCat 2.0[67]. Additional statistical analyses, including Fisher's exact test, were conducted in RStudio. The software and R packages employed for processing sequencing data and performing differential analyses in ATAC-seq and RNA-seq datasets are detailed in the Methods section. All experiments were carried out with at least two biological replicates, with similar results. Details regarding the number of replicates, sample size, types of statistical analyses, p-value cutoffs, and raw data are provided in the corresponding figure legends and/or *source.data*.

References

1. Calabrese, E.J. (2014). Hormesis: a fundamental concept in biology. Microb. Cell *1*, 145–149. https://doi.org/10.15698/mic2014.05.145.

2. Gems, D., and Partridge, L. (2008). Stress-Response Hormesis and Aging: "That which Does Not Kill Us Makes Us Stronger." Cell Metab. *7*, 200–203. https://doi.org/10.1016/j.cmet.2008.01.001.

3. Mattson, M.P. (2008). Hormesis defined. Ageing Res. Rev. *7*, 1–7. https://doi.org/10.1016/j.arr.2007.08.007.

4. Cypser, J.R., and Johnson, T.E. (2002). Multiple stressors in Caenorhabditis elegans induce stress hormesis and extended longevity. J. Gerontol. A. Biol. Sci. Med. Sci. *57*, B109-114. https://doi.org/10.1093/gerona/57.3.b109.

5. Shama, S., Lai, C.-Y., Antoniazzi, J.M., Jiang, J.C., and Jazwinski, S.M. (1998). Heat Stress-Induced Life Span Extension in Yeast. Exp. Cell Res. *245*, 379–388. https://doi.org/10.1006/excr.1998.4279.

6. Yokoyama, K., Fukumoto, K., Murakami, T., Harada, S., Hosono, R., Wadhwa, R., Mitsui, Y., and Ohkuma, S. (2002). Extended longevity of *Caenorhabditis elegans* by knocking in extra copies of hsp70F, a homolog of mot-2 (mortalin)/mthsp70/Grp75. FEBS Lett. *516*, 53–57. https://doi.org/10.1016/S0014-5793(02)02470-5.

7. Cypser, J.R., Tedesco, P., and Johnson, T.E. (2006). Hormesis and aging in *Caenorhabditis elegans*. Exp. Gerontol. *41*, 935–939. https://doi.org/10.1016/j.exger.2006.09.004.

8. Le Bourg, É., Valenti, P., Lucchetta, P., and Payre, F. (2001). Effects of mild heat shocks at young age on aging and longevity in Drosophila melanogaster. Biogerontology *2*, 155–164. https://doi.org/10.1023/A:1011561107055.

9. Hercus, M.J., Loeschcke, V., and Rattan, S.I.S. (2003). Lifespan extension of Drosophila melanogaster through hormesis by repeated mild heat stress. Biogerontology *4*, 149–156. https://doi.org/10.1023/a:1024197806855.

10. Rattan, S.I.S. (2005). Hormetic Modulation of Aging and Longevity by Mild Heat Stress. Dose-Response *3*, dose-response.003.04.008. https://doi.org/10.2203/dose-response.003.04.008.

11. Rattan, S.I.S., Fernandes, R.A., Demirovic, D., Dymek, B., and Lima, C.F. (2008). Heat Stress and Hormetin-Induced Hormesis in Human Cells: Effects on Aging, Wound Healing, Angiogenesis, and Differentiation. Dose-Response *7*, 90–103. https://doi.org/10.2203/dose-response.08-014.Rattan.

12. Mane, N.R., Gajare, K.A., and Deshmukh, A.A. (2018). Mild heat stress induces hormetic effects in protecting the primary culture of mouse prefrontal cerebrocortical neurons from neuropathological alterations. IBRO Rep. *5*, 110–115. https://doi.org/10.1016/j.ibror.2018.11.002.

13. Verbeke, P., Deries, M., Clark, B.F.C., and Rattan, S.I.S. (2002). Hormetic action of mild heat stress decreases the inducibility of protein oxidation and glycoxidation in human fibroblasts. Biogerontology *3*, 117–120. https://doi.org/10.1023/a:1015284119308.

14. Laukkanen, T., Kunutsor, S.K., Khan, H., Willeit, P., Zaccardi, F., and Laukkanen, J.A. (2018). Sauna bathing is associated with reduced cardiovascular mortality and improves risk prediction in men and women: a prospective cohort study. BMC Med. *16*, 219. https://doi.org/10.1186/s12916-018-1198-0.

15. Patrick, R.P., and Johnson, T.L. (2021). Sauna use as a lifestyle practice to extend healthspan. Exp. Gerontol. *154*, 111509. https://doi.org/10.1016/j.exger.2021.111509.

16. Lithgow, G.J., White, T.M., Melov, S., and Johnson, T.E. (1995). Thermotolerance and extended life-span conferred by single-gene mutations and induced by thermal stress. Proc. Natl. Acad. Sci. U. S. A. *92*, 7540–7544.

17. McColl, G., Rogers, A.N., Alavez, S., Hubbard, A.E., Melov, S., Link, C.D., Bush, A.I., Kapahi, P., and Lithgow, G.J. (2010). Insulin-like Signaling Determines Survival During Stress via Post Transcriptional Mechanisms in C. elegans. Cell Metab. *12*, 260–272. https://doi.org/10.1016/j.cmet.2010.08.004.

18. Butov, A., Johnson, T., Cypser, J., Sannikov, I., Volkov, M., Sehl, M., and Yashin, A. (2001). Hormesis and debilitation effects in stress experiments using the nematode worm *Caenorhabditis*

elegans: the model of balance between cell damage and HSP levels. Exp. Gerontol. *37*, 57–66. https://doi.org/10.1016/S0531-5565(01)00161-9.

19. Kumsta, C., Chang, J.T., Schmalz, J., and Hansen, M. (2017). Hormetic heat stress and HSF-1 induce autophagy to improve survival and proteostasis in C. elegans. Nat. Commun. *8*, 14337. https://doi.org/10.1038/ncomms14337.

20. Zhang, B., Xiao, R., Ronan, E.A., He, Y., Hsu, A.-L., Liu, J., and Xu, X.Z.S. (2015). Environmental Temperature Differentially Modulates *C. elegans* Longevity through a Thermosensitive TRP Channel. Cell Rep. *11*, 1414–1424. https://doi.org/10.1016/j.celrep.2015.04.066.

21. Zhou, L., He, B., Deng, J., Pang, S., and Tang, H. (2019). Histone acetylation promotes long-lasting defense responses and longevity following early life heat stress. PLOS Genet. *15*, e1008122. https://doi.org/10.1371/journal.pgen.1008122.

22. Kovács, D., Biró, J.B., Ahmed, S., Kovács, M., Sigmond, T., Hotzi, B., Varga, M., Vincze, V.V., Mohammad, U., Vellai, T., et al. (2024). Age-dependent heat shock hormesis to HSF-1 deficiency suggests a compensatory mechanism mediated by the unfolded protein response and innate immunity in young Caenorhabditis elegans. Aging Cell *23*, e14246. https://doi.org/10.1111/acel.14246.

23. Jiang, W.I., De Belly, H., Wang, B., Wong, A., Kim, M., Oh, F., DeGeorge, J., Huang, X., Guang, S., Weiner, O.D., et al. (2024). Early-life stress triggers long-lasting organismal resilience and longevity via tetraspanin. Sci. Adv. *10*, eadj3880. https://doi.org/10.1126/sciadv.adj3880.

24. Xu, F., Li, R., von Gromoff, E.D., Drepper, F., Knapp, B., Warscheid, B., Baumeister, R., and Qi, W. (2023). Reprogramming of the transcriptome after heat stress mediates heat hormesis in Caenorhabditis elegans. Nat. Commun. *14*, 4176. https://doi.org/10.1038/s41467-023-39882-8.

25. Eder, M., Martin, O.M.F., Oswal, N., Sedlackova, L., Moutinho, C., Carmen-Fabregat, A.D., Bravo, S.M., Sebé-Pedrós, A., Heyn, H., and Stroustrup, N. (2024). Systematic mapping of organism-scale gene-regulatory networks in aging using population asynchrony. Cell *187*, 3919-3935.e19. https://doi.org/10.1016/j.cell.2024.05.050.

26. Bazopoulou, D., Knoefler, D., Zheng, Y., Ulrich, K., Oleson, B.J., Xie, L., Kim, M., Kaufmann, A., Lee, Y.-T., Dou, Y., et al. (2019). Developmental ROS individualizes organismal stress resistance and lifespan. Nature *576*, 301–305. https://doi.org/10.1038/s41586-019-1814-y.

27. Schreiner, W.P., Pagliuso, D.C., Garrigues, J.M., Chen, J.S., Aalto, A.P., and Pasquinelli, A.E. (2019). Remodeling of the Caenorhabditis elegans non-coding RNA transcriptome by heat shock. Nucleic Acids Res. *47*, 9829–9841. https://doi.org/10.1093/nar/gkz693.

28. Starks, R.R., Biswas, A., Jain, A., and Tuteja, G. (2019). Combined analysis of dissimilar promoter accessibility and gene expression profiles identifies tissue-specific genes and actively repressed networks. Epigenetics Chromatin *12*, 16. https://doi.org/10.1186/s13072-019-0260-2.

29. Calabrese, E.J., Bachmann, K.A., Bailer, A.J., Bolger, P.M., Borak, J., Cai, L., Cedergreen, N., Cherian, M.G., Chiueh, C.C., Clarkson, T.W., et al. (2007). Biological stress response terminology: Integrating the concepts of adaptive response and preconditioning stress within a hormetic dose–response framework. Toxicol. Appl. Pharmacol. *222*, 122–128. https://doi.org/10.1016/j.taap.2007.02.015.

30. Kim, Y., and Sun, H. (2007). Functional genomic approach to identify novel genes involved in the regulation of oxidative stress resistance and animal lifespan. Aging Cell *6*, 489–503. https://doi.org/10.1111/j.1474-9726.2007.00302.x.

31. Wang, A., Song, Z., Zhang, X., Xiao, L., Feng, Y., Qi, C., Zhang, G., Bai, J., Liu, Y., Sun, T., et al. (2023). MARS1 mutations linked to familial trigeminal neuralgia via the integrated stress response. J. Headache Pain *24*, 4. https://doi.org/10.1186/s10194-022-01537-2.

32. Lindquist, S., and Craig, E.A. (1988). THE HEAT-SHOCK PROTEINS. Annu. Rev. Genet. *22*, 631–677. https://doi.org/10.1146/annurev.ge.22.120188.003215.

33. Morimoto, R.I. (2011). The heat shock response: systems biology of proteotoxic stress in aging and disease. Cold Spring Harb. Symp. Quant. Biol. *76*, 91–99. https://doi.org/10.1101/sqb.2012.76.010637.

34. Shi, Y., Mosser, D.D., and Morimoto, R.I. (1998). Molecularchaperones as HSF1-specific transcriptional repressors. Genes Dev. *12*, 654–666.

35. Malinow, R.A., Ying, P., Koorman, T., Boxem, M., Jin, Y., and Kim, K.W. (2019). Functional Dissection of C. elegans bZip-Protein CEBP-1 Reveals Novel Structural Motifs Required for Axon Regeneration and Nuclear Import. Front. Cell. Neurosci. *13*. https://doi.org/10.3389/fncel.2019.00348.

36. Lin, X.-X., Sen, I., Janssens, G.E., Zhou, X., Fonslow, B.R., Edgar, D., Stroustrup, N., Swoboda, P., Yates, J.R., Ruvkun, G., et al. (2018). DAF-16/FOXO and HLH-30/TFEB function as combinatorial transcription factors to promote stress resistance and longevity. Nat. Commun. *9*, 4400. https://doi.org/10.1038/s41467-018-06624-0.

37. Kasper, D.M., Wang, G., Gardner, K.E., Johnstone, T.G., and Reinke, V. (2014). The C. elegans SNAPc Component SNPC-4 Coats piRNA Domains and Is Globally Required for piRNA Abundance. Dev. Cell *31*, 145–158. https://doi.org/10.1016/j.devcel.2014.09.015.

38. Weng, C., Kosalka, J., Berkyurek, A.C., Stempor, P., Feng, X., Mao, H., Zeng, C., Li, W.-J., Yan, Y.-H., Dong, M.-Q., et al. (2019). The USTC co-opts an ancient machinery to drive piRNA transcription in C. elegans. Genes Dev. *33*, 90–102. https://doi.org/10.1101/gad.319293.118.

39. Hou, X., Zhu, C., Xu, M., Chen, X., Sun, C., Nashan, B., Guang, S., and Feng, X. (2022). The SNAPc complex mediates starvation-induced trans-splicing in *Caenorhabditis elegans*. J. Genet. Genomics *49*, 952–964. https://doi.org/10.1016/j.jgg.2022.02.024.

40. Frost, F.G., Morimoto, M., Sharma, P., Ruaud, L., Belnap, N., Calame, D.G., Uchiyama, Y., Matsumoto, N., Oud, M.M., Ferreira, E.A., et al. (2023). Bi-allelic SNAPC4 variants dysregulate global alternative splicing and lead to neuroregression and progressive spastic paraparesis. Am. J. Hum. Genet. *110*, 663–680. https://doi.org/10.1016/j.ajhg.2023.03.001.

41. Belicard, T., Jareosettasin, P., and Sarkies, P. (2018). The piRNA pathway responds to environmental signals to establish intergenerational adaptation to stress. BMC Biol. *16*, 103. https://doi.org/10.1186/s12915-018-0571-y.

42. Batista, P.J., Ruby, J.G., Claycomb, J.M., Chiang, R., Fahlgren, N., Kasschau, K.D., Chaves, D.A., Gu, W., Vasale, J.J., Duan, S., et al. (2008). PRG-1 and 21U-RNAs interact to form the piRNA

complex required for fertility in C. elegans. Mol. Cell *31*, 67–78. https://doi.org/10.1016/j.molcel.2008.06.002.

43. Tepper, R.G., Ashraf, J., Kaletsky, R., Kleemann, G., Murphy, C.T., and Bussemaker, H.J. (2013). PQM-1 Complements DAF-16 as a Key Transcriptional Regulator of DAF-2-Mediated Development and Longevity. Cell *154*, 676–690. https://doi.org/10.1016/j.cell.2013.07.006.

44. McGhee, J.D., Fukushige, T., Krause, M.W., Minnema, S.E., Goszczynski, B., Gaudet, J., Kohara, Y., Bossinger, O., Zhao, Y., Khattra, J., et al. (2009). ELT-2 is the predominant transcription factor controlling differentiation and function of the C. elegans intestine, from embryo to adult. Dev. Biol. *327*, 551–565. https://doi.org/10.1016/j.ydbio.2008.11.034.

45. Wiesenfahrt, T., Berg, J.Y., Osborne Nishimura, E., Robinson, A.G., Goszczynski, B., Lieb, J.D., and McGhee, J.D. (2016). The function and regulation of the GATA factor ELT-2 in the C. elegans endoderm. Development *143*, 483–491. https://doi.org/10.1242/dev.130914.

46. Kerry, S., TeKippe, M., Gaddis, N.C., and Aballay, A. (2006). GATA Transcription Factor Required for Immunity to Bacterial and Fungal Pathogens. PLOS ONE *1*, e77. https://doi.org/10.1371/journal.pone.0000077.

47. Chuang, P.-T., Albertson, D.G., and Meyer, B.J. (1994). DPY-27: A chromosome condensation protein homolog that regulates C. elegans dosage compensation through association with the X chromosome. Cell *79*, 459–474. https://doi.org/10.1016/0092-8674(94)90255-0.

48. Daugherty, A.C., Yeo, R.W., Buenrostro, J.D., Greenleaf, W.J., Kundaje, A., and Brunet, A. (2017). Chromatin accessibility dynamics reveal novel functional enhancers in C. elegans. Genome Res. *27*, 2096–2107. https://doi.org/10.1101/gr.226233.117.

49. Hoeppner, D.J., Spector, M.S., Ratliff, T.M., Kinchen, J.M., Granat, S., Lin, S.-C., Bhusri, S.S., Conradt, B., Herman, M.A., and Hengartner, M.O. (2004). *eor-1* and *eor-2* are required for cell-specific apoptotic death in *C. elegans*. Dev. Biol. *274*, 125–138. https://doi.org/10.1016/j.ydbio.2004.06.022.

50. Zhang, Z., Liu, L., Twumasi-Boateng, K., Block, D.H.S., and Shapira, M. (2017). FOS-1 functions as a transcriptional activator downstream of the C. elegans JNK homolog KGB-1. Cell. Signal. *30*, 1–8. https://doi.org/10.1016/j.cellsig.2016.11.010.

51. Fletcher, M., Tillman, E.J., Butty, V.L., Levine, S.S., and Kim, D.H. (2019). Global transcriptional regulation of innate immunity by ATF-7 in C. elegans. PLOS Genet. *15*, e1007830. https://doi.org/10.1371/journal.pgen.1007830.

52. Shaulian, E., and Karin, M. (2002). AP-1 as a regulator of cell life and death. Nat. Cell Biol. *4*, E131–E136. https://doi.org/10.1038/ncb0502-e131.

53. Gerke, P., Keshet, A., Mertenskötter, A., and Paul, R.J. (2014). The JNK-Like MAPK KGB-1 of Caenorhabditis Elegans Promotes Reproduction, Lifespan, and Gene Expressions for Protein Biosynthesis and Germline Homeostasis but Interferes with Hyperosmotic Stress Tolerance. Cell. Physiol. Biochem. *34*, 1951–1973. https://doi.org/10.1159/000366392.

54. Lynch, C.J., Richart, L., and Serrano, M. (2024). A pattern emerges in chromatin aging: AP-1 steals the show. Cell Metab. *36*, 1639–1641. https://doi.org/10.1016/j.cmet.2024.07.015.

55. Patrick, R., Naval-Sanchez, M., Deshpande, N., Huang, Y., Zhang, J., Chen, X., Yang, Y., Tiwari, K., Esmaeili, M., Tran, M., et al. (2024). The activity of early-life gene regulatory elements is hijacked in aging through pervasive AP-1-linked chromatin opening. Cell Metab. *36*, 1858-1881.e23. https://doi.org/10.1016/j.cmet.2024.06.006.

56. Meyer, B.J. (2022). The X chromosome in *C. elegans* sex determination and dosage compensation. Curr. Opin. Genet. Dev. *74*, 101912. https://doi.org/10.1016/j.gde.2022.101912.

57. Anderson, E.C., Frankino, P.A., Higuchi-Sanabria, R., Yang, Q., Bian, Q., Podshivalova, K., Shin, A., Kenyon, C., Dillin, A., and Meyer, B.J. (2019). X Chromosome Domain Architecture Regulates Caenorhabditis elegans Lifespan but Not Dosage Compensation. Dev. Cell *51*, 192-207.e6. https://doi.org/10.1016/j.devcel.2019.08.004.

58. Davis, P., Zarowiecki, M., Arnaboldi, V., Becerra, A., Cain, S., Chan, J., Chen, W.J., Cho, J., da Veiga Beltrame, E., Diamantakis, S., et al. (2022). WormBase in 2022—data, processes, and tools for analyzing Caenorhabditis elegans. Genetics *220*, iyac003. https://doi.org/10.1093/genetics/iyac003.

59. Han, S.K., Lee, D., Lee, H., Kim, D., Son, H.G., Yang, J.-S., Lee, S.-J.V., and Kim, S. (2016). OASIS 2: online application for survival analysis 2 with features for the analysis of maximal lifespan and healthspan in aging research. Oncotarget *7*, 56147–56152. https://doi.org/10.18632/oncotarget.11269.

60. Kamath, R.S., and Ahringer, J. (2003). Genome-wide RNAi screening in *Caenorhabditis elegans*. Methods *30*, 313–321. https://doi.org/10.1016/S1046-2023(03)00050-1.

61. Rual, J.-F., Ceron, J., Koreth, J., Hao, T., Nicot, A.-S., Hirozane-Kishikawa, T., Vandenhaute, J., Orkin, S.H., Hill, D.E., van den Heuvel, S., et al. (2004). Toward Improving Caenorhabditis elegans Phenome Mapping With an ORFeome-Based RNAi Library. Genome Res. *14*, 2162–2168. https://doi.org/10.1101/gr.2505604.

62. Chen, R.A.-J., Down, T.A., Stempor, P., Chen, Q.B., Egelhofer, T.A., Hillier, L.W., Jeffers, T.E., and Ahringer, J. (2013). The landscape of RNA polymerase II transcription initiation in C. elegans reveals promoter and enhancer architectures. Genome Res. *23*, 1339–1347. https://doi.org/10.1101/gr.153668.112.

63. Jänes, J., Dong, Y., Schoof, M., Serizay, J., Appert, A., Cerrato, C., Woodbury, C., Chen, R., Gemma, C., Huang, N., et al. (2018). Chromatin accessibility dynamics across C. elegans development and ageing. eLife *7*, e37344. https://doi.org/10.7554/eLife.37344.

64. Bailey, T.L., Johnson, J., Grant, C.E., and Noble, W.S. (2015). The MEME Suite. Nucleic Acids Res. *43*, W39–W49. https://doi.org/10.1093/nar/gkv416.

65. Rauluseviciute, I., Riudavets-Puig, R., Blanc-Mathieu, R., Castro-Mondragon, J.A., Ferenc, K., Kumar, V., Lemma, R.B., Lucas, J., Chèneby, J., Baranasic, D., et al. (2024). JASPAR 2024: 20th anniversary of the open-access database of transcription factor binding profiles. Nucleic Acids Res. *52*, D174–D182. https://doi.org/10.1093/nar/gkad1059.

66. Weirauch, M.T., Yang, A., Albu, M., Cote, A.G., Montenegro-Montero, A., Drewe, P., Najafabadi, H.S., Lambert, S.A., Mann, I., Cook, K., et al. (2014). Determination and inference of eukaryotic transcription factor sequence specificity. Cell *158*, 1431–1443. https://doi.org/10.1016/j.cell.2014.08.009.

67. Holdorf, A.D., Higgins, D.P., Hart, A.C., Boag, P.R., Pazour, G.J., Walhout, A.J.M., and Walker, A.K. (2020). WormCat: An Online Tool for Annotation and Visualization of Caenorhabditis elegans Genome-Scale Data. Genetics *214*, 279–294. https://doi.org/10.1534/genetics.119.302919.

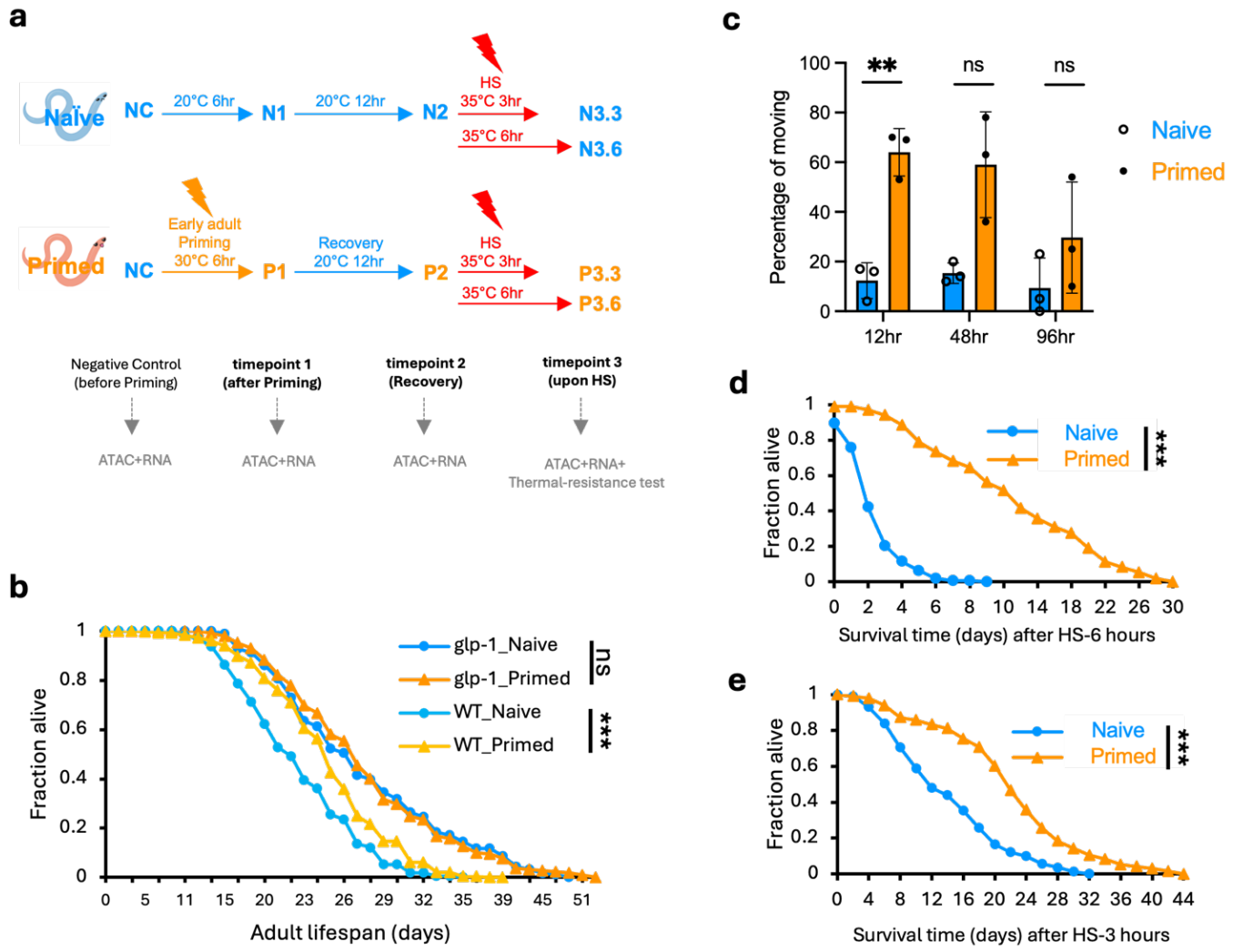

Figure 1: Our heat hormesis regimen enhances thermal-resistance and extends lifespan.

(a) Schematic of heat hormesis regimen and timepoints of multiomics studies: The primed group was exposed to mild heat stress at 30°C for 6 hours (priming) during early adult stage, followed by 12 hours of recovery at 20°C. The naive group was incubated at 20°C concurrently. Both groups were subjected to subsequent heat shock (HS) challenges at the indicated temperature and duration. Negative control (NC) timepoint was collected before priming. For both naive and primed groups, timepoint 1 (T1) was collected after priming (N1 and P1), timepoint 2 (T2) after recovery (N2 and P2), and timepoints 3 (T3)

after 3 hours or 6 hours of HS (N3.3, P3.3, N3.6, P3.6). (**b)** Lifespan of *glp-1(ts)* or WT worms with or without priming was assessed at 20°C. The figure represents combined data from four independent experiments (N=4). Survival curves for *glp-1*_Naive, *glp-1*_Primed, WT_Naive, WT_Primed are shown. (**c)** Thermal-resistance of *glp-1(ts)* (*e2141* temperature sensitive allele) was assessed based on percentage of worms moving post-HS. The y-axis represents average results from three separate experiments, each with different recovery period between priming and subsequent HS challenge. Recovery times and HS conditions varied due to the ease of experimental design: 12 hours recovery followed by 10 hours HS at 35°C; 48 hours recovery followed by 5 hours HS at 37°C; 96 hours recovery followed by 5 hours HS at 37°C. Movement was scored 15 hours post-HS. (N = 3). (**d-e)** Thermal-resistance was assessed based on survival of *glp-1(ts)* worms after being subjected to 6 hours (**d**) or 3 hours (**e**) of HS at 35°C, following a 12-hour recovery from priming. The figure represents combined data from three independent experiments (N=3). A 2-tailed unequal variances t-test was conducted to compare differences between naive and primed groups in (c). ** Indicates $p < 0.01$, *** Indicates $p < 0.001$. Details can be found in *source.data.*

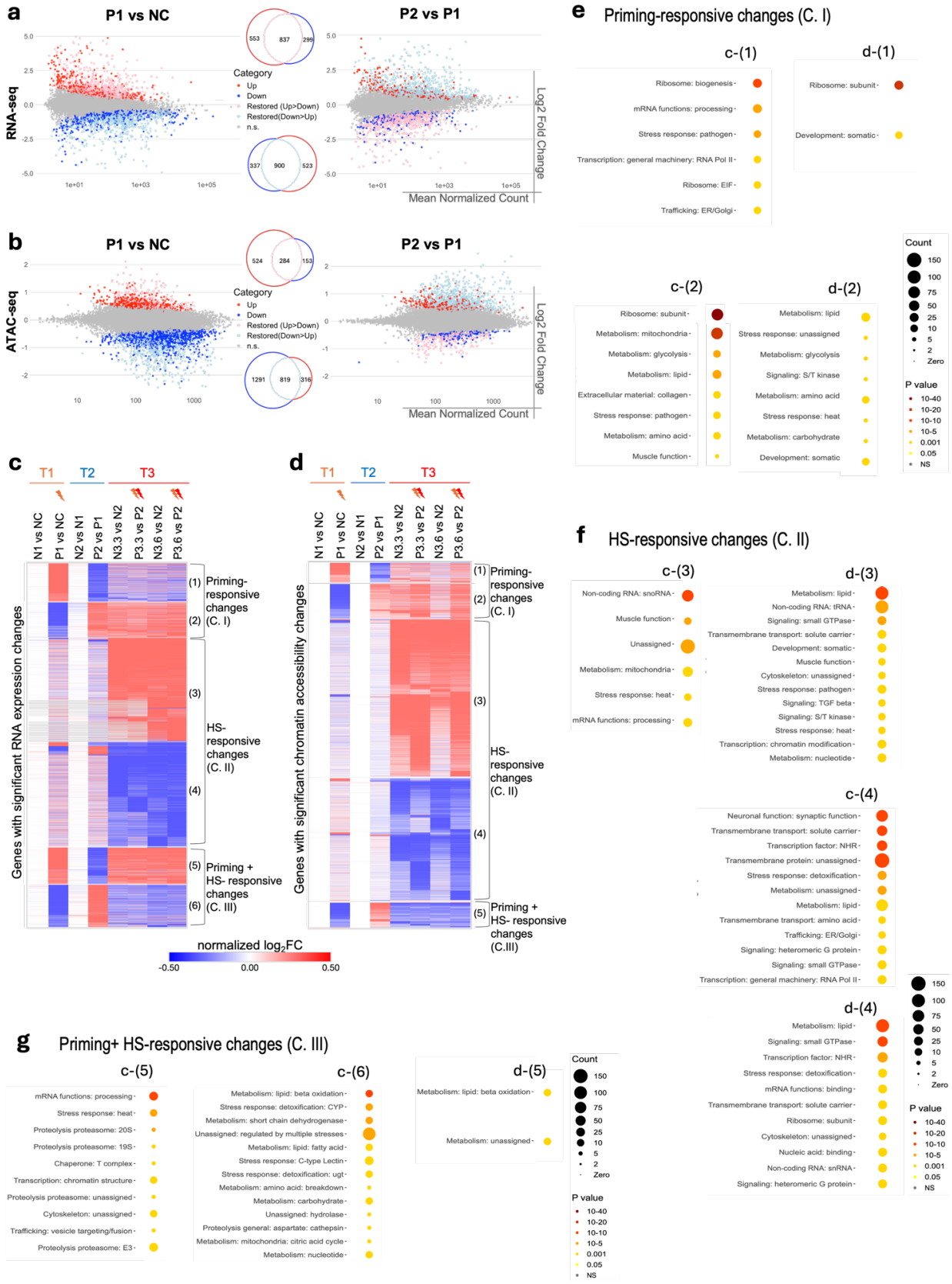

Figure 2: Priming-responsive changes largely restored after recovery and are distinct from Heat Shock-responsive changes in gene expression and chromatin accessibility.

MA plots display log2 fold chang (FC) of RNA expression **(a)** from RNA-seq and chromatin accessibility **(b)** from ATAC-seq, comparing P1 vs NC (left panel) and P2 vs P1 (right panel). Differential analyses were conducted using DESeq2. Significant changes (p-adj < 0.05) are marked in red for upregulation (log2FC > 0) and in blue for downregulation (log2FC < 0), while unchanged are marked in grey (p-adj >= 0.05). Significantly upregulated changes in P1vs NC (red) that overlap with significantly downregulated changes in P2 vs P1 (blue) are highlighted in pink and labeled as 'Restored (Up > Down)'. Conversely, changes that are significantly downregulated in P1 vs NC (blue) that overlap with significantly upregulated in P2 vs P1 (red) are highlighted in light blue and labeled as 'Restored (Down > Up)'. The number of significant and restored genes **(a)** and peaks **(b)** are summarized and color-coded in Venn Diagrams in the middle panel. Heatmaps display significant genes with RNA expression changes **(c),** or chromatin accessibility changes **(d)** identified across the indicated comparisons, clustered by K-mean analysis using Morpheus. The colors represent normalized log2FC. The clusters in the heatmaps are arranged to parallelly present shared patterns between changes in RNA expression and chromatin accessibility. Heatmaps are classified into three categories. Category I (C. I), Priming-responsive changes: Involved clusters (1) and (2) in both **(c), (d)**; Category II (C. I), HS-responsive changes: Involved clusters (3) and (4) in both **(c), (d)**; Category III (C. III), Priming + HS-responsive changes: Involved clusters (5) and (6) in **(c)**, and cluster 5 in **(d)** (Details of the gene lists in the heatmaps can be found in the Supplementary Data 1 & 2). Wormcat GO enrichment analysis for genes in C. I **(e)** and C. II **(f)**, C. III **(g)**. Wormcat p-values are determined by one-side Fisher test with FDR correction. Gene and peak lists, and Wormcat outputs, are provided in the Supplementary Data 3.

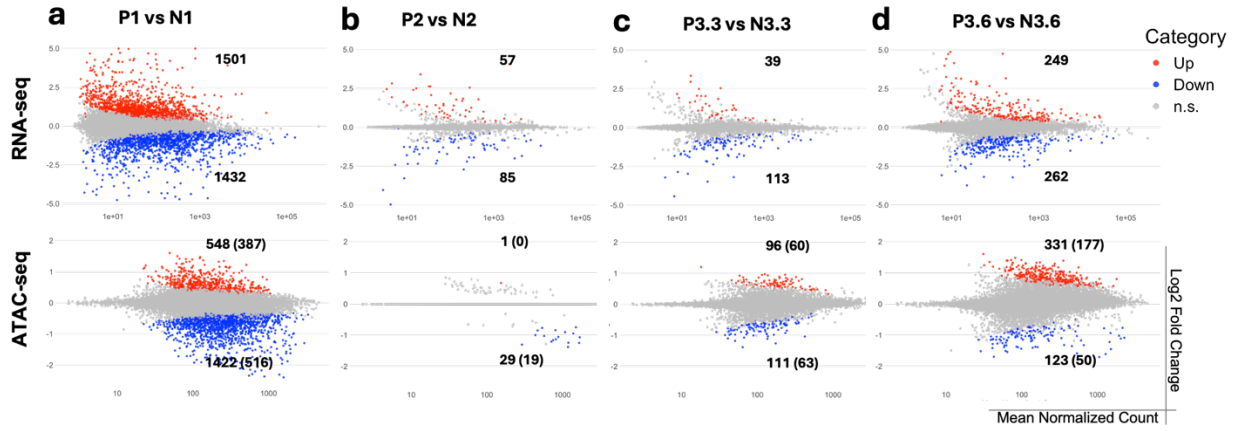

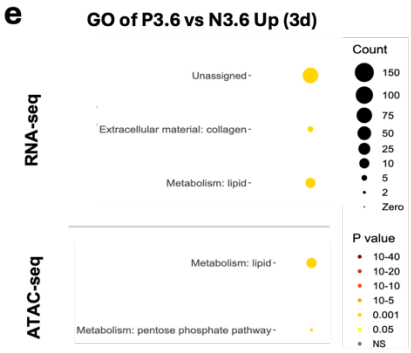

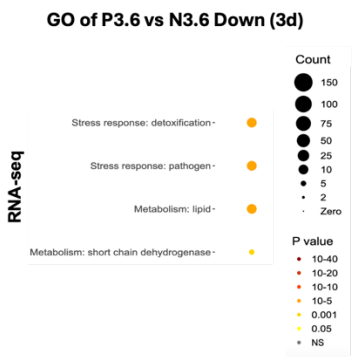

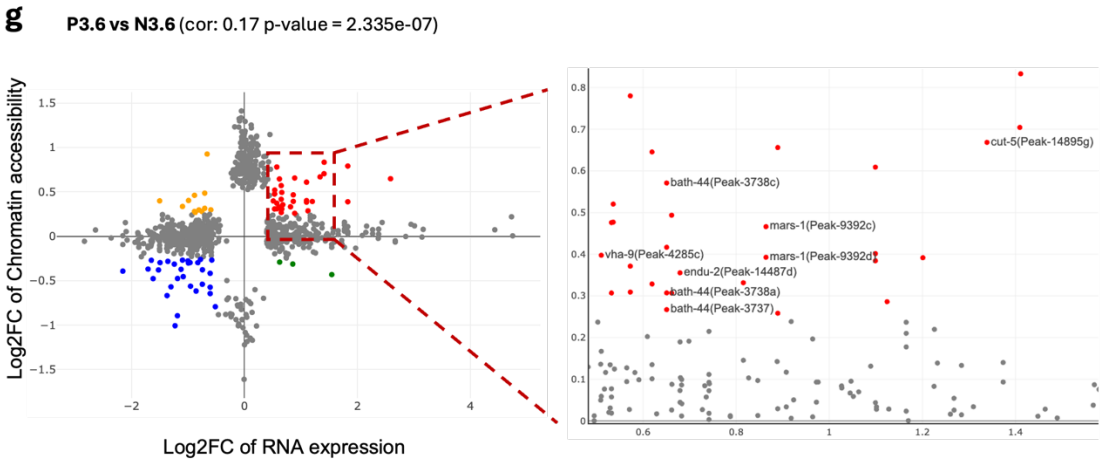

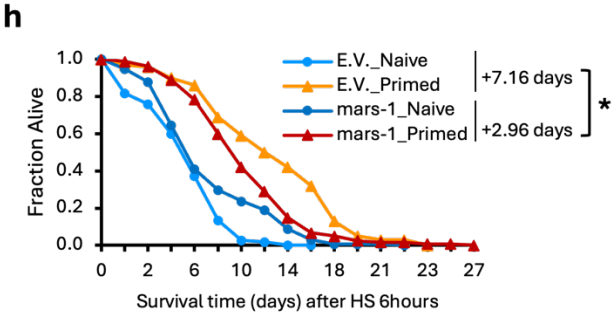

Figure 3: Differences in gene expression or chromatin accessibility in primed and naive worms likely contribute to the protective effects of heat hormesis.

MA plots display log2FC in gene expression (RNA-seq, top panel) and chromatin accessibility (ATAC-seq, bottom panel) for comparisons between primed and naive groups at the indicated timepoints: after priming **(a)**, after recovery **(b)**, after a 3-hour HS **(c)** and a 6-hour HS **(d)**. Significant changes (p-adj < 0.05) are marked in red for upregulation (log2FC > 0), in blue for downregulation (log2FC < 0), and non-significant changes in grey (p-adj >= 0.05). Number of significant genes and peaks (with associated genes in brackets) are indicated. Wormcat GO enrichment analysis for genes upregulated **(e)** or downregulated **(f)** in primed compared to naive groups after a 6-hour HS. Details are provided in the *source.data* and Supplementary Data 3. **(g)** Scatter plot displays genes with significant changes identified in RNA expression or chromatin accessibility after a 6-hour HS, with correlated changes between RNA-seq and ATAC-seq data highlighted according to defined criteria: log2FC RNA expression > 0.5, < -0.5; log2FC Chromatin accessibility > 0.25, < -0.25. The area showing genes upregulated in both RNA expression and chromatin accessibility (red) is zoomed out in the right panel. The five candidate genes (and their associated peaks) selected for RNAi testing are labeled. **(h)** Thermal-resistance was assessed based on the survival of *glp-1(ts)* worms treated with the indicated RNAi or empty vector (E.V.) after being subjected to our heat hormesis regimen and challenged with a 6-hour HS. Survival curves represent combined data from three independent experiments (N=3). The survival extension rate is calculated to quantify the increase in mean survival days in primed versus naive group in each independent experiment. A paired two-tailed t-test evaluates the significant reduction in survival extension upon gene silencing, showing a significant decrease in the *mars-1* RNAi group compared to the E.V. control. *Indicates $p < 0.05$. N=3. Details can be found in the Supplementary Data 4.

Candidates	P1 vs NC	P3.6 vs P2	(P1 vs NC) & (P3.6 vs P2) intersect	P1 vs N1	P3.6 vs N3.6
cebp-1	RNA: up	RNA: up (2000bp)		RNA: up	
		ATAC: up	ATAC: up	ATAC: up	
snpc-4		RNA: up			
	ATAC: up			ATAC: up	
hlh-30	RNA: down (2000bp)	RNA: up (2000bp)			
	ATAC: down	ATAC: up			ATAC: up
hsf-1 (CIS-BP)		RNA: up	RNA: up		
		ATAC: up, down			
elt-2	RNA: down			RNA: down	RNA: down
elt-6	RNA: down			RNA: down	RNA: down
pqm-1	RNA: down			RNA: down	RNA: down
dpy-27	ATAC: down			ATAC: down	ATAC: down
fos-1		ATAC: up			
atf-7		ATAC: up			

Table 1: Candidate transcription factors predicted by motif analysis and tested by RNAi

The table shows the transcription factor candidates predicted by motif analysis that have been tested by RNAi, with at least two independent experiments.

Promoter regions of genes associated with significant changes in RNA expression from RNA-seq and DNA regions spanning significantly changed peaks from ATAC-seq were subjected to motif analysis. Motif candidates were primarily selected from the JASPAR database, except for the HSF-1 motif, which is from CIS-BP database. Motifs identified from RNA-seq data were primarily enriched in the 500bp upstream promoter region of the TSS, unless indicated as 2000bp. The complete list of all significantly enriched motifs (Q value < 0.05) is shown in *source.data*. The table is color-coded into three groups: Motifs enriched based on both ATAC-seq and RNA-seq results (pink); Motifs enriched based on only RNA-seq (green); Motifs enriched based on only ATAC-seq results (blue). In addition to HSF-1, three candidates from each group were selected for RNAi screening if they were repeatedly identified in different significant lists, RNAi constructs were available, and the candidate factor has been implicated in stress response and longevity according to the literature.

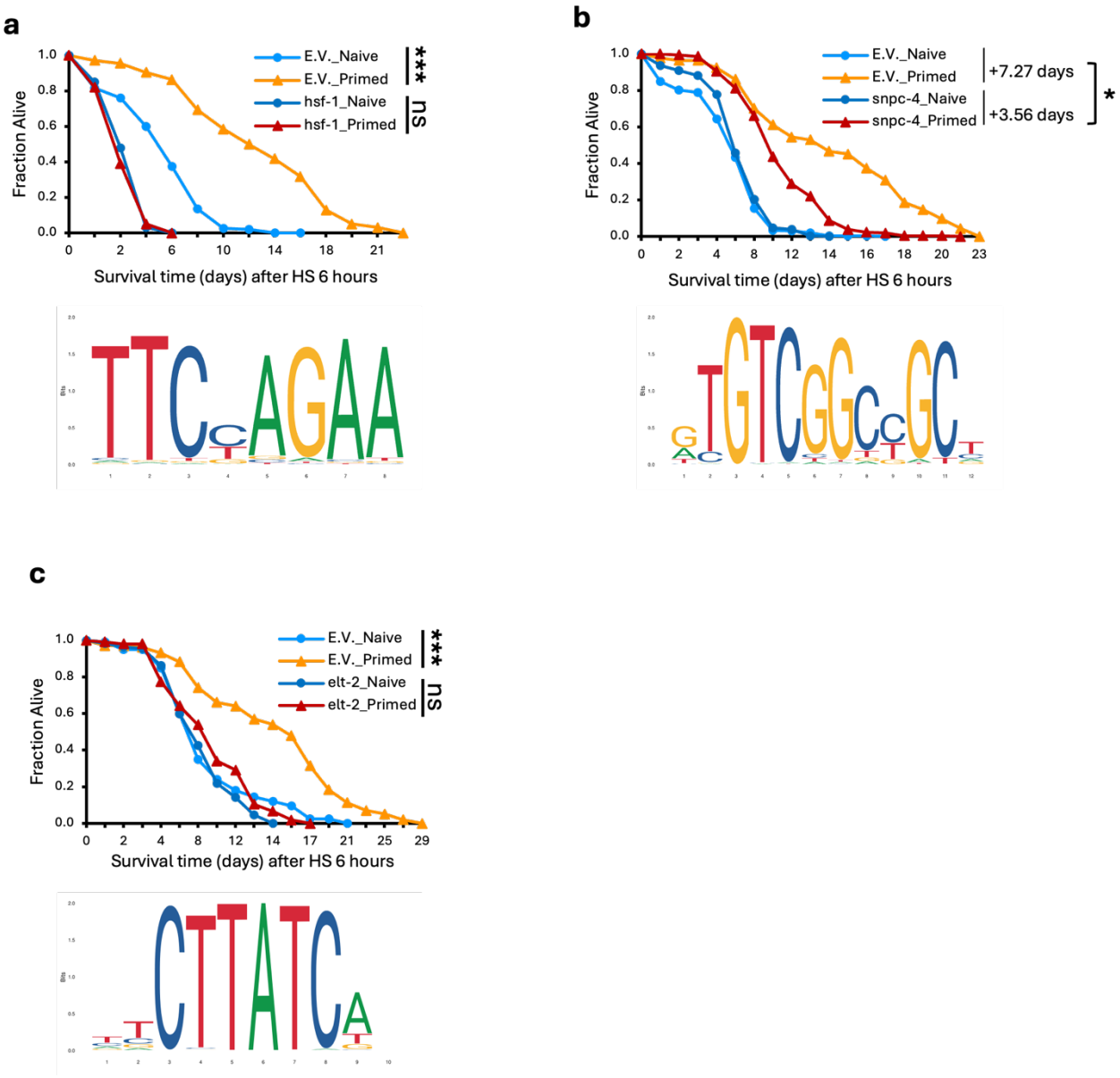

Figure 4: Motif analysis unveils regulators in heat hormesis.

Thermal-resistance was assessed based on survival of *glp-1(ts)* mutant worms treated with the indicated RNAi and after being subjected to our hormesis regimen and challenged with a 6-hour HS. Survival curves represent combined data from multiple independent experiments (N) for *glp-1*_Naive or *glp-1*_Primed treated with empty vector (E.V.) control RNAi or *hsf-1* RNAi **(a; N=3)**, *snpc-4* RNAi **(b; N=4)**, *elt-2* RNAi **(c; N=2)**. RNAi targeting *hsf-1***(a)** and *elt-2* **(c)** completely abolished the enhanced survival to heat in primed groups, as indicated by significant differences between primed and naive groups in the

E.V. control but not in the RNAi-treated groups. *** Indicates $p < 0.001$. For the *snpc-4* **(b)** RNAi, which partially compromised the enhanced survival to heat in primed groups, the survival extension rate is calculated, and the increase in mean survival days in primed worms relative to naive worms is shown. Statistical analyses were conducted to determine whether the survival extension rate is significant based on four independent experiments (N=4). * Indicates $p < 0.05$. Motif logos were obtained from databases and are displayed.